Microbiome

RESEARCH

Open Access

Diet prevents the expansion of segmented filamentous bacteria and ileo-colonic inflammation in a model of Crohn's disease

Amira Metwaly[1], Jelena Jovic[1], Nadine Waldschmitt[1], Sevana Khaloian[1], Helena Heimes[1], Deborah Häcker[1], Mohamed Ahmed[1], Nassim Hammoudi[2,3], Lionel Le Bourhis[3], Aida Mayorgas[4], Kolja Siebert[5], Marijana Basic[6], Tobias Schwerd[5], Matthieu Allez[2,3], Julian Panes[4], Azucena Salas[4], André Bleich[6], Sebastian Zeissig[7], Pamela Schnupf[8], Fabio Cominelli[9] and Dirk Haller[1,10*]

Abstract

Background Crohn's disease (CD) is associated with changes in the microbiota, and murine models of CD-like ileo-colonic inflammation depend on the presence of microbial triggers. Increased abundance of unknown Clostridiales and the microscopic detection of filamentous structures close to the epithelium of *Tnf* $^{\Delta ARE}$ mice, a mouse model of CD-like ileitis pointed towards segmented filamentous bacteria (SFB), a commensal mucosal adherent bacterium involved in ileal inflammation.

Results We show that the abundance of SFB strongly correlates with the severity of CD-like ileal inflammation in two mouse models of ileal inflammation, including *Tnf* $^{\Delta ARE}$ and SAMP/Yit mice. SFB mono-colonization of germ-free *Tnf* $^{\Delta ARE}$ mice confirmed the causal link and resulted in severe ileo-colonic inflammation, characterized by elevated tissue levels of *Tnf* and *Il-17A*, neutrophil infiltration and loss of Paneth and goblet cell function. Co-colonization of SFB in human-microbiota associated *Tnf* $^{\Delta ARE}$ mice confirmed that SFB presence is indispensable for disease development. Screening of 468 ileal and colonic mucosal biopsies from adult and pediatric IBD patients, using previously published and newly designed human SFB-specific primer sets, showed no presence of SFB in human tissue samples, suggesting a species-specific functionality of the pathobiont. Simulating the human relevant therapeutic effect of exclusive enteral nutrition (EEN), EEN-like purified diet antagonized SFB colonization and prevented disease development in *Tnf* $^{\Delta ARE}$ mice, providing functional evidence for the protective mechanism of diet in modulating microbiota-dependent inflammation in IBD.

Conclusions We identified a novel pathogenic role of SFB in driving severe CD-like ileo-colonic inflammation characterized by loss of Paneth and goblet cell functions in *Tnf* $^{\Delta ARE}$ mice. A purified diet antagonized SFB colonization and prevented disease development in *Tnf* $^{\Delta ARE}$ mice in contrast to a fiber-containing chow diet, clearly demonstrating the important role of diet in modulating a novel IBD-relevant pathobiont and supporting a direct link between diet and microbial communities in mediating protective functions.

Keywords Crohn's disease, Segmented filamentous bacteria, Purified diet, *Tnf* $^{\Delta ARE}$ mice, Inflammation, Pathobiont, IBD

*Correspondence:
Dirk Haller
dirk.haller@tum.de
Full list of author information is available at the end of the article

Introduction

CD is one of the two main subtypes of inflammatory bowel diseases (IBD) that affect the gastrointestinal tract and is characterized by patchy transmural inflammation along the small intestine, predominantly affecting the terminal ileum and proximal colon. Accumulating evidence proved that CD is a multifactorial disease, mainly driven by complex interactions between genetics, environmental factors, gut microbiota, and immune responses [1, 2]. To date, more than 70 CD and 241 IBD susceptibility loci have been identified via large-scale genome-wide association studies (GWAS) [3, 4]. Of note, many of these genetic risk loci are involved in immune pathways linked to microbial sensing and signaling, lack of adaptive mechanisms (e.g., interleukin (IL) 23/T helper (Th) 17 pathway) in the regulation of immune activation, autophagy, and Paneth cell function [5–7]. However less than 30% of the heritability to CD is explained by known genetic variants, suggesting that microbial triggers play a dominant role in disease etiology. Perturbations of gut microbiome structure and function (also referred to as dysbiosis) are causally linked to a distortion of microbe-host homeostasis, leading to the development of chronic intestinal inflammation, such as Crohn's disease (CD) and Ulcerative colitis (UC) [8–11]. In this context, work from us and others clearly demonstrated that the presence of commensal bacteria is required to induce inflammation in several mouse models of IBD, while germ-free (GF) counterparts remained completely disease-free [12–16].

The *Tnf* $^{\Delta ARE}$ CD mouse model is one of the very few models that develop intestinal inflammation resembling the transmural ileal disease phenotype frequently seen in CD patients [17–20]. We previously showed that GF *Tnf* $^{\Delta ARE}$ mice are completely disease-free, and the transfer of disease-associated intestinal microbiota induced CD-like inflammation [12]. Further, mucosa-associated microbial communities of *Tnf* $^{\Delta ARE}$ mice were characterized by the expansion of segmented filamentous bacteria (SFB) [13], a spore-forming, anaerobic symbiotic commensal bacteria of the phylum Firmicutes. SFB were shown to attach to the ileal mucosa at the time of weaning and are responsible for controlling immune cell maturation, including IL17-producing innate and adaptive lymphocytes [21–24]. Although first reported over 100 years ago, SFB can only be cultured for a limited amount of time in vitro in an epithelial cell-SFB co-culturing system [24]. Using 16S rRNA gene sequence analysis, it has been shown that SFB of mice, rats, and chickens represent a cluster within the *Clostridium* genus [25]. First evidence for the presence of SFB in humans was based on the visualization of a tentative SFB organism adherent to ileal tissue biopsies by light microscopy [26] and this was later supported in samples from patients with ulcerative colitis [27]. More recently, 16S rRNA gene sequences of SFB were reported in human samples using SFB-specific PCR primers, where SFB sequences were found in 55 fecal samples [28] and in one ileostomy sample [29]. Further, Finotti et al. [30] reported detection of SFB in tissue biopsies from the terminal ileum of UC patients. In mice, SFB adhesion to intestinal epithelial cells contributes to the mucosal immune system function by inducing the differentiation of Th17, production of secretory immunoglobulin A (IgA), and the secretion of antimicrobial peptides (AMPs) [31–33]. Similar associations were observed in luminal fluids from children, suggesting comparable immunomodulatory effects of SFB growth in early age of human individuals [34]. Although the role of SFB in humans to induce antigen specific Th17 cells remains largely unknown, they appear to play an important role in modulating the gut immune response in mouse models of ileal inflammation. The regulatory mechanisms controlling SFB growth remain unclear.

Diet is proposed to be an essential factor in IBD that targets inflammation-related mechanisms in the host, either directly or indirectly via changes in the structure and function of the intestinal microbiota [35, 36]. Studies on various patient cohorts proposed specific dietary components to be associated with IBD, including higher consumption of sugar and animal fat as well as a reduced vegetable intake [37, 38]. Early studies in the 1980s suggested that dietary composition might be an important determinant of the presence of SFB in the small intestine of mice; however, the dietary components responsible were not identified [39–41].

Here, we identified a novel pathogenic role of SFB in driving severe CD-like ileo-colonic inflammation characterized by loss of Paneth and goblet cell functions in *Tnf* $^{\Delta ARE}$ mice. A purified diet antagonized SFB colonization and prevented disease development in *Tnf* $^{\Delta ARE}$ mice in contrast to a fiber-containing chow diet, clearly demonstrating the important role of diet in modulating a novel IBD-relevant pathobiont. Taken together, we showed that dietary intervention using EEN-like purified diet in a murine model of CD prevented pathobiont-mediated intestinal inflammation, supporting a direct link between diet and microbial communities in mediating protective functions.

Methods

Ethics statement

Mouse experiments and the treatment protocols were approved by the Committee on Animal Health and Care of the local government body of the state of Upper Bavaria (Regierung von Oberbayern; approvals number (55.2-1-54-2531-99-13, 55.2-1-54-2532-133-2014 and 55.2-2532.Vet_02-17-104) and performed in compliance

with the EEC recommendations for the care and use of Lab. Animals. (European Communities Council Directive of 24 November 1986 (86/609/EEC). Animals were housed in the germ-free (GF) mouse facility at the Technical University of Munich (School of Life Sciences). IBD Patients were recruited at the Department of Gastroenterology, Hospital Clinic Barcelona, at Hospital San Louis in Paris and at Dr. von Hauner Children's Hospital in Munich. The study was approved by the corresponding hospital ethics committee. All patients provided written informed consent.

Animal experiments

Tnf $^{\Delta ARE}$ mice and wild-type (WT) control littermates were imported from Case Western Reserve University in Cleveland and housed under germ-free (GF) conditions. Eight-weeks old GF mice were colonized with specific-pathogen-free (SPF)-derived WT cecal microbiota and maintained under SPF housing conditions. Co-housing experiments were performed with 8-week-old female *Tnf* $^{\Delta ARE}$ and WT littermates and female SFB mono-colonized NOD-SCID mice. Monocolonization of ARE and WT mice with SFB was performed either by breeding of mice with SFB-mono-colonized WT mothers or by oral gavage of gut content from mono-colonized NOD-SCID mice into 8-week-old *Tnf* $^{\Delta ARE}$ mice and controls. Monocolonization of mice with *Alistipes*, *B. adolescentis* L2-32, *Alistipes* sp., *Escherichia coli* LF82, and *Lactobacillus murinus* was done by oral gavage of freshly prepared inoculum from over-night bacterial cultures, whereas colonization with minimal mouse microbial consortium was performed by oral gavage of previously prepared cryo stocks of mixed bacterial cultures in 20% glycerol (v/v) on three consecutive days within 1 week. Humanization experiment was performed by transferring human fecal microbiota derived from a CD patient recruited in Barcelona and who received hematopoietic stem cell transplantation [15, 42] to *Tnf* $^{\Delta ARE}$ and WT mice at the age of 8 weeks. Preparation of human fecal material for inoculation in germ-free mice was done under anaerobic conditions and using reduced PBS (PBS supplemented with 0.05% L-cysteine-HCl) in an anaerobic chamber (atmosphere, 90% N2, 5% CO2, and 5% H2) and vortexed at room temperature for 5 min. The fecal suspension was allowed to settle by gravity for 5 min to exclude residual particulate matter. The clear supernatant was transferred under anaerobic conditions into an anaerobic crimped tube, which was transferred to the gnotobiotic facility. Each germ-free recipient mouse received 100 µL of the suspension via oral gavage using a 20-Gauge gavage needle (Fine Science Tools). Mice were sacrificed 4 weeks after colonization. WT and *Tnf* $^{\Delta ARE}$ mice were placed on purified diets (Ssniff E15000, Germany), enriched with fiber (Ssniff S5745-E907, Germany) at 7 or 9 weeks of age. SFB mono-colonization was performed by transplantation of gut content of mono-colonized NOD-SCID mice at 8 weeks of age, and mice were sampled at 12 weeks of age. Detailed information about diet ingredients is summarized in Supplementary Table S1.

Germ-free WT and IL-10-deficient ($Il10^{-/-}$) mice on 129Sv/Ev background were kept at the gnotobiology core facility of the Institute for food and health, Technical University Munich, Germany. Mono-colonization of $Il10^{-/-}$ and WT mice with SFB was performed by oral gavage of gut content from mono-colonized NOD-SCID mice into 8 weeks old $Il10^{-/-}$ mice and WT controls.

SAMP1Yi/Fc (SAMP) mice

Ten- and > 24-week-old specific-pathogen-free (SPF) SAMP and age/sex matched AKR/J mice were used. Mice were kept on a 12-h light/dark cycle in a species-appropriate temperature/humidity-controlled room and maintained in AAALAC-accredited Animal Research Center rooms at Case Western Reserve University (CWRU).

Housing of germ-free mice

GF mice were kept at the gnotobiology core facility of the Institute for food and health, Technical University Munich, Germany. GF mice were housed in flexible film isolators ventilated via HEPA-filtered air at 22 ± 1 °C with a 12-h light/dark cycle. Before experiments, littermates were combined and randomly assigned to treatment groups. A maximum of 5 mice are housed per cage (floor area ~ 540 cm^2). Mice received standard Chow, purified or fiber-rich purified diet (autoclaved V1124-300; Ssniff, Soest, Germany) and autoclaved water ad libitum.

CD patients and control subjects

Mucosal biopsies for SFB quantification were collected from three IBD patient cohorts enrolled in Barcelona, Paris, and Munich Supplementary Table S2.

Spanish (HSCT) cohort

Enrolled patients were in follow-up for CD following treatment with autologous hematopoietic stem cell transplantation (AHSCT). Ileal ($n = 44$) and colonic biopsies ($n = 78$) from CD patients were included in the analysis. CD patients recruited fulfilled the previously described inclusion criteria [15, 42–44]. Biopsies were immediately frozen at − 80 °C for PCR analysis).

French (biotherapy) cohort

This longitudinal study comprised patients with IBD (CD and UC) who are treated with anti-TNF and other biotherapy drugs and recruited in Paris. Ileal ($n = 43$) and colonic biopsies ($n = 143$) from CD and UC patients were included in the analysis.

German pediatric cohort

This longitudinal prospective study comprised children with IBD and were recruited in Munich. Ileal ($n = 72$) and colonic biopsies ($n = 80$) were included in the analysis.

Bacterial cultivation and inoculation of mice

All individual bacterial isolates used in the mouse experiments were deposited at the German Collection of Microorganisms and Cell Cultures (DSMZ), except for *Bifidobacterium adolescentis* L2-32 (gift of Harry Flint, University of Aberdeen, United Kingdom) and reference strain *Escherichia coli* LF82 (generously supplied by Arlette Darfeuille-Michaud, Université of Auvergne, France). *Lactobacillus murinus* (DSM #28683, *E. coli LF8*2 (adherent invasive *Escherichia coli* derived from a chronic ileal lesion in a CD patient) and *Alistipes* sp. (DSM #27924) were cultivated in Wilkins-Chalgren anaerobe broth (WCA, Oxoid) that was prepared in Hungate tube flushed with nitrogen. Purity of bacterial strains was controlled by microscopic evaluation following a standard Gram staining procedure. GF age matched ARE and WT mice were inoculated with 1×10^8 CFU by oral gavage and sacrificed 4 weeks after colonization. MIBAC–Minimal mouse Bacteriome is a consortium of 7 bacteria that acts as a proxy model of a complex mouse gut microbiota (unpublished). It was selected based on prevalence and abundance values in mouse gut using omics datasets. The final composition of MIBAC is as follows: *Clostridium ramosum*, *Paraclostridium bifermentans*, *Enterococcus hirae*, *Enterorhabdus mucosicola*, *Escherichia coli*, *Lactobacillus murinus*, and *Parabacteroides goldsteinii*.

Bacterial DNA extraction from feces

Fecal pellets were resuspended in 600 µl DNA stabilization solution (STRATEC biomedical), 400 µl Phenol:Chloroform:IsoAmyl alcohol (25:24:1; Sigma-Aldrich), and 500 mg autoclaved zirconia/silica beads (0.1 mm; Roth). Bacterial cells were mechanically disrupted by using a FastPrep®-24 (MP Biomedicals) followed by a heat treatment for 8 min at 95 °C and centrifugation with 15000×*g* for 5 min at 4 °C. Supernatants were treated with RNase (0.1 µg/µl; VWR International) for 30 min at 37 °C. DNA was purified by using the gDNA clean-up kit (Macherey-Nagel). DNA concentrations and purity were checked using NanoDrop® (Thermo Fisher Scientific), and DNA integrity was checked by gel electerophoresis (0.5%, 100V, 45 min). Samples were immediately used or stored at − 20 C for long-term storage.

DNA extraction from tissue biopsy

DNA was extracted from biopsies by using the NucleoSpin® Tissue kit (Machery-Nagel). Briefly, tissue biopsies were resuspended in 180 µl sterile filtered lysis buffer (20 mM Tris/HCl; 2 mM EDTA; 1 % Triton X-100 (pH 8) and supplemented with freshly prepared lysozyme solution (20 mg/ml). Tissue suspensions were incubated in a thermoshaker (37 °C, 30 min, 950 rpm). Afterwards, Proteinase K (10mg/ml) was added, and the suspension was vortexed vigorously and incubated in a thermoshaker (56 °C, 1–3 h, 950 rpm) until complete lysis of tissue pieces. Further purification steps were performed by using the NucleoSpin® Tissue kit following the manufacturer's instructions.

High throughput 16S ribosomal RNA (rRNA) gene sequencing and microbiome profiling

Library preparation and sequencing were performed as described in detail previously. In brief, the V3-V4 regions of the 16S rRNA gene was amplified (10 × 15 cycles for fecal samples, 15 × 15 cycles for tissue biopsies) by using previously described two-step protocol [45] using forward and reverse primers 341F-785R 34. Purification of amplicons was performed by using the AMPure XP system (Beckmann). Sequencing was performed with pooled samples in paired-end modus (PE275) using a MiSeq system (Illumina, Inc.) according to the manufacturer's instructions and 25% (v/v) PhiX standard library. Processing of raw reads was performed by using IMNGS pipeline based on the UPARSE approach [46]. Sequences were demultiplexed, trimmed to the first base with a quality score < 3 and then paired. Sequences with less than 300 and more than 600 nucleotides and paired reads with an expected error > 3 were excluded from the analysis. Trimming of remaining reads was done by trimming 5 nucleotides on each end to avoid GC bias and non-random base composition. A table of zOTUs is constructed by considering all reads before any quality filtering. ZOTUs (zero-radius OTUs) are valid operational taxonomic units that provide the maximum possible biological resolution compared to conventional 97% OTUs. Since using 97% identity may merge phenotypically different strains with distinct sequences into a single cluster, zOTUs are found to be superior to conventional OTU clusters ([47]. Taxonomy assignment was performed at 80% confidence level using the SILVA ribosomal RNA

gene database project [48]. Analysis was performed in R programming environment by using Rhea R-package [49]. Sequencing depth was assessed by using rarefaction curves, and samples with low quality were removed or re-sequenced. Diversity between groups was analyzed by using ß-diversity based on generalized UniFrac distances. Alpha-diversity was assessed based on species richness and Shannon effective diversity. *P* values were calculated by using ANOVA on ranks and corrected for multiple comparisons according to the Benjamini-Hochberg method. Only taxa with a prevalence of at least 30% samples in one given group were considered for statistical analysis.

Reverse transcriptase-polymerase chain reaction

Total RNA from total ileal, cecal, and colonic tissue was isolated by using the NucleoSpin RNAII kit (Macherey-Nagel GmbH) according to manufacturer's instructions. Complementary DNA was synthetized from 500 ng total RNA by using random hexamers and moloney murine leukemia virus (M-MLV) reverse transcriptase (RT) Point Mutant Synthesis System (Promega). Quantification was performed by using the LightCycler 480 Universal Probe Library System (Roche). Following primer sequences and respective probes () were used: *Tnf* for_*5′-TGCCTATGTCTCAGCCTCTTC-3′*, *rev_5′-GAGGCCATTTGGGAACTTCT-3′* (49), *Gapdh* for_*5′-CACACCCATCACAAACATGG-3′*, *rev_5′-GCCAAAAGGGTCATCATCTC-3′* (29), *Il-17A* for_*5′-AGGGATATCTATCAGGGTCTTCATT-3′*, *rev_5'-TGTGAAGGTCAACCTCAAAGTC-3′* (50), *Ifng* for_*5′-AGCGTTCATTGTCTCAGAGCTA-3′*, *rev_5′-CCTTTGGACCCTCTGACTTG-3′* (63), *Ang4* for_*5′-CGTAGGAATTTTTCGTACCTTTCA-3′*, *rev_5′-CCCCAGTTGGAGGAAAGC-3′* (106); *Defa-5* for_*5'-CAGAGCCGATGGTTGTCAT-3′*, *rev_5′-TTTTGGGACCTGCAGAAATC-3′* (84), *Reg3b* for_*5′-TCATCACGTCATTGTTACTCCA-3′*, *rev_5′-TGGATTGGGCTCCATGAC-3′* (10), *Muc2* for_*5′-GGTCTGGCAGTCCTCGAA-3′*, *rev_5′-GGCAGTACAAGAACCGGAGT-3′* (66). Quantification of SFB in fecal mouse content was performed using the MasterMix SensiFAST™ SYBR (BIOLINE) and specific primer pair for_*5′ -GACGCTGAGGCATGAGAGCAT-3′* , *rev_5′-GACGGCACGGATTGTTATTCA*-3' [50]. Quantification of SFB in human tissue biopsies was performed using the MasterMix SensiFAST™ SYBR (BIOLINE) and 3 different primer sets: *for_5'-TGTGGGTTGTGAATAGCAAT-3′* [30], *rev_5′-GCGAGCTTCCCTCATTACAAGG-3′* , *for_5′ -AGGAGGAGTCTGCGGCACATTAGC-3′* [51, 52] ,*rev_5′* TCCCCACTGCTGCCTCCCGTAG-*3′* [53, 54] and for,_ *5′-TGTAGGTTGTGAAGAACAAT-3′*, *rev_ 5′-GCGAGCTTCCCTCATTACAAGG-3′* (modified primer sequences, unpublished data, Pamela Schnupf).

Gel electrophoresis

Agarose gel 1 v/w % containing 0.001% Gelred (InvivoGen) was prepared by using Tris Acetate-EDTA buffer. qPCR amplicons were separated at 100 V for 1 h following DNA band visualization under UV light.

Isolation of immune cell population from lamina propria

Lamina propria-resident immune cells from small intestine were isolated by digesting intestinal tissue with Collagenase VIII (Sigma-Aldrich). Shortly, Payer's patches were removed, and epithelial layer was dissociated by incubating tissue pieces twice in 2mM EDTA/PBS for 20 min at 37 °C with shaking (180 rpm). Afterwards, single cell suspension was prepared by digesting small intestinal tissue in complete RPMI medium (10% FCS, 1% P/S, 1% Glu) containing Collagenase VIII (0.6 mg/ml) for approximately 15 min at 37 °C with shaking (180 rpm). Lamina propria-resident immune cells from large intestine were isolated by digesting intestinal tissue with Collagenase D (Roche), Collagenase V (Sigma-Aldrich), Dispase I (Gibco), and DNase I (Roche). Here, epithelial cells were removed by incubating tissue pieces twiese in 2mM EDTA/PBS for 15 min at 37 °C with shaking (180 rpm). Next, single cell suspension was prepared by digesting large intestinal tissue in complete RPMI medium (10% FCS, 1% P/S, 1% Glu) containing Collagenase D (1.25 mg/ml), Collagenase V (0.85 mg/ml), Dispase I (1 mg/ml), and DNase (30 U/ml) for a maximum of 45 min at 37 °C with shaking (180 rpm). Cell number of single cell suspensions (2% FCS/PBS) were assessed, and cells were kept at 4 °C for immediate flow cytometry analysis.

Flow cytometry analysis

Cells were stained and subsequently analyzed by using a LSRII system (BD Biosciences). Dead cells were excluded with the Zombie GreenTM or Zombie NIRTM Fixable Viability Kit (BioLegend). Allophycocyanin-Cy7-conjugated anti-CD3 (17A2), PE-Cy7-conjugated anti-CD4 (RM4-5), PE-Cy7-conjugated anti-CD11b (M1/70), PE-conjugated anti-CD45 (30-F11), PerCP/Cyanine5.5-conjugated anti-mouse I-A/I-E (M5/114.15.2), Allophycocyanin-Cy7-conjugated anti-Ly6C (HK1.4), Allophycocyanin-conjugated anti-Ly6G (1A8), and PerCP/Cyanine5.5-conjugated anti-CD3 (17A2) were from BioLegend, Allophycocyanin-conjugated anti-CD25 (PC61.5), PE-conjugated anti-Foxp3 (FJK-16s), PE-Cy7-conjugated anti-IL17 (eBio17B7), and Allophycocyanin-conjugated anti-IFN gamma (XMG1.2)

were from Thermo Fisher Scientific, and FITC-conjugated anti-CD4 (RM4-5) was from BD Biosciences. FcR block was done by using FcR blocking reagent, mouse (Miltenyi Biotec) and intracellular staining was performed by using eBioscience™ Foxp3/Transcription Factor Staining Buffer Set (Thermo Fisher Scientific).

Tissue fixation and staining procedures

Intestinal specimens were fixed in 4% formaldehyde/PBS for 24 h at RT, subsequently dehydrated (Leica TP1020), and embedded in paraffin (McCormick; Leica EG1150C). Five-micrometer-thick tissue sections were prepared, deparaffinized, and hematoxylin and eosin (H&E) staining was performed by using a Leica ST5020 Multistainer system. For periodic acid Schiff (PAS) and Alcian blue (AB) staining, formalin-fixed paraffin-embedded (FFPE) tissue sections were deparaffinized and rehydrated. Alcian blue solution for acidic mucins (1% volume/volume in 3% acetic acid, pH 2.5) was applied for 15 min. Tissue sections were incubated with periodic acid solution (0.5% volume/volume) for 5 min and co-staining with Schiff's reagent (Sigma-Aldrich) for neutral mucins was performed for 10 min. Nuclei were counterstained with hematoxylin for 1 min. Numbers of goblet cells (GC) were calculated as a total number per area of interest. Images were acquired by using the Digital microscope M8 and MicroPoint software (PreciPoint GmbH). For immunofluorescent (IF) staining, 3.5 µm-thick tissue sections were placed on SuperFrost PlusTM slides (Thermo Fisher Scientific), deparaffinized (Leica ST5020), and rehydrated. Antigen retrieval was performed in 10 mM sodium citrate buffer (pH 6.0) by steaming sections in a microwave oven (900 Watt) for 23 min. Slides were rinsed with H2O and sections were blocked for 1h with blocking buffer containing the serum (5%). Primary antibodies against E-Cadherin (ab76055, 1:300, Abcam) and Lysozyme (A0099, 1:1000, DAKO, Agilent) were directly applied and incubated overnight at 4 °C. Fluorescently labelled secondary antibodies anti-rabbit (A10040, A31571, 1:200, Life Technologies) and anti-mouse (A11001, 1:200, Life Technologies) were incubated light-protected for 1 h at RT. DAPI (Sigma-Aldrich) was added for nuclear staining. Tissue sections were mounted (BIOZOL Diagnostica) and analyzed by using the Flouview FV10i microscope (Olympus).

Fluorescent in situ hybridization

Dissected, intact ileal and colonic tubes were fixed in Carnoy solution (60% dry MeOH, 30% dry chloroform, 10% acetic acid) overnight at RT. Dehydration of samples was performed by washes in dry MeOH, 100% EtOH, xylene/100% EtOH (1:1), and xylene. Dehydrated tissue was submerged in melted paraffin for 20 minutes and embedded. Nine-µm-thick tissue sections were deparaffinized, rehydrated, and fixed in 10% formalin before permeabilizing in a lysozyme solution (40 mg/mL lysozyme in a filter-sterilized 2 mmol/L Tris/2 mmol/L EDTA/1.2% volume/volume Triton-X100 buffer) for 45 min at 37 °C. Tissue sections were incubated with Cy5-conjugated bacterial probe EUB338 (5′-GCTGCCTCCCGTAGGAGT-3′) overnight at 46 °C. Sections were co-stained with anti-MUC2 (H-300, 1:100, Santa Cruz Biotechnology) for 1 h at RT following 30 min of incubation with secondary antibody (1:200, A11034, Life Technologies) and nuclei were visualized by using DAPI (Sigma-Aldrich).

Histological scoring system

Scoring of H&E stained tissue sections was performed blindly by evaluating lamina propria mononuclear cell infiltration, crypt hyperplasia, goblet cell depletion, and architectural distortion [55, 56]. Grade of inflammation is reflected by total scores from 0 to 12.

Results

Severity of CD-like inflammation correlates with SFB abundance in Tnf $^{\Delta ARE}$ and SAMP/YitFc mice

Our previous data showed that GF *Tnf* $^{\Delta ARE}$ mice are completely disease-free, and only upon the transfer of complex microbial communities derived from inflamed *Tnf* $^{\Delta ARE}$ mice, they develop intestinal inflammation. Increased abundance of unknown Clostridiales [12] and the microscopic detection of rod-like structures in close proximity to the epithelium of *Tnf* $^{\Delta ARE}$ mice [13] pointed towards the relevance of SFB. A colony of non-inflamed GF *Tnf* $^{\Delta ARE}$ mice and littermate WT controls (F0) was colonized with cecal content of SPF-housed WT mice having SFB counts reduced to undetectable levels. Mice were subsequently transferred to SPF housing for breeding (F1, F2) and monitoring of inflammation. At 18 weeks of age, the newly introduced *Tnf* $^{\Delta ARE}$ mice gradually developed ileal inflammation**.** The number of responder mice, however, significantly increased over the following two breeding generations. Similarly, subsequent generations of SPF-housed *Tnf* $^{\Delta ARE}$ mice exhibited varying severity of ileal inflammation independent of cage and litter effect (Supplementary Figure S1B). As we previously reported, three inflammatory phenotypes upon bacterial colonization could be observed in *Tnf* $^{\Delta ARE}$ mice, including severe inflammation (referred to as responders, R, inflammation score > 4), mild inflammation (referred to as low responders, LR, inflammation score < 4), as well as no inflammation (referred to as non-responders, NR, inflammation score 0) [12] (Supplementary Figure S1C, D). We investigated the progression of ileal inflammation as well as SFB abundance over time.

Our data show that shortly after weaning all 3–4 weeks old *Tnf* $^{\Delta ARE}$ mice were disease-free and started to show mild tissue pathology at the age of 8 weeks (Fig. 1A). With regard to the SFB growth, both 3–4 weeks old *Tnf* $^{\Delta ARE}$ mice and WT controls revealed high SFB titers in cecal content, which subsequently declined below detectable levels in aging littermate WT controls, while it only has continuously decreased in non-inflamed NR *Tnf* $^{\Delta ARE}$ mice (Fig. 1B). Histopathological evaluation showed tissue pathology to be restricted to the ileal compartment (Fig. 1C). To visualize bacterial structures in ileal tissue sections of non-inflamed (NR) and inflamed (R) *Tnf* $^{\Delta ARE}$ mice (F1), we performed fluorescence in situ hybridization (FISH) by staining ileum sections with bacteria domain-specific (EUB338) probes. Microscopic examination showed detection of filamentous bacteria close to the intestinal epithelium of responder mice (Fig. 1D). The inflammation in ileal tissue of responder mice is characterized by significantly enhanced *Tnf* and *Il17A* transcript levels compared to non-inflamed WT controls (Fig. 1E). A correlation analysis on the full cohort of 18 weeks old *Tnf* $^{\Delta ARE}$ mice (NR, LR, R) resulted in significant association between SFB abundance in intestinal content and severity of ileal tissue pathology ($p < 0.0001$, $r = 0.5998$) (Fig. 1F). Next to *Tnf* $^{\Delta ARE}$ mice, we quantified SFB abundances in SAMP1/YitFc mice, a unique mouse model that spontaneously develop CD-like "cobblestone" ileitis with 100% penetrance and within a well-defined time course (pre-ileitis, disease induction, and chronic ileitis) [57]. Similarly, a correlation analysis on a cohort of SAMP1/YitFc mice showed significant association between SFB abundance in fecal pellets and severity of ileal tissue pathology ($p < 0.01$, $r = 0.4827$) (Fig. 1G), demonstrating a potential relevance of SFB as an important specific pathogenic factor for ileal inflammation.

To examine SFB-driven alterations in complex microbial ecosystems, 8 weeks old, SPF-housed *Tnf* $^{\Delta ARE}$ mice and WT controls with low SFB counts in fecal content were co-housed with SFB-mono-colonized NOD-SCID mice for 10 weeks (Supplementary Figure S1A). Fecal pellets were collected weekly and analyzed using 16S rRNA gene amplicon sequencing. After 10 weeks of co-housing, all *Tnf* $^{\Delta ARE}$ mice showed significant signs of inflammation, while WT mice remained disease-free. To assess how SFB affects the microbiota, we compared gut microbiota composition between WT and *Tnf* $^{\Delta ARE}$ mice (Supplementary Figure 1E). 16S microbial profiling revealed a substantial change in gut microbiota composition, characterized by significant increase in the relative abundance of *Alistipes* species in the inflamed *Tnf* $^{\Delta ARE}$ mice compared to WT controls. In contrast, increased abundance of *Lactobacillus* was evident for WT mice (Supplementary Figure S1F). Intriguingly, subsequent mono-colonization of GF *Tnf* $^{\Delta ARE}$ mice with *Alistipes* failed to induce any inflammatory responses and/or ileal pathology (Supplementary Figure S1G). We additionally tested the impact of monocolonizing *Tnf* $^{\Delta ARE}$ mice with the human adherent-invasive *Escherichia coli* LF82 or *Lactobacillus spp*. and both showed no impact of these bacteria in inducing inflammation in *Tnf* $^{\Delta ARE}$ mice. We next hypothesized that a simplified consortium of selected mouse gut bacterial would mimic the complex intestinal microbiota and be a sufficient trigger for ileal inflammation in *Tnf* $^{\Delta ARE}$ mice. To test this hypothesis, we colonized *Tnf* $^{\Delta ARE}$ mice and WT controls with a simplified minimal mouse bacterial, which comprises 7 bacterial strains (*Clostridium ramosum, Paraclostridium bifermentans, Enterococcus hirae, Enterorhabdus mucosicola, Escherichia coli, Lactobacillus murinus*, and *Parabacteroides goldsteinii*) (Supplementary Table S3). These were selected based on their prevalence and abundance values in the mouse gut samples and all were previously characterized as either mouse-enriched, prevalent, or dominant [58]. However, and despite of the increased bacterial complexity, this bacterial consortium failed to induce inflammation in *Tnf* $^{\Delta ARE}$ mice as shown by histopathological assessment of inflammation in ileal, cecal, and colonic tissue (Supplementary Figure S1G), as well as TNF gene expression analysis in ileal tissue (Ct-value >

(See figure on next page.)

Fig. 1 SFB abundance correlates with ileitis severity in SPF-house *Tnf* $^{\Delta ARE}$ mice. **A** Ileitis scores of SPF-housed *Tnf* $^{\Delta ARE}$ mice at the age of 3–4, 8, 12, and 18 weeks of age. Color-code represents severity of inflammation as described above. Cecal content of SPF-housed WT mice with undetectable SFB counts was introduced into germ-free *Tnf* $^{\Delta ARE}$ mice and littermate WT controls. **B** Quantitative analysis of SFB abundance in *Tnf* $^{\Delta ARE}$ and matching WT mice overtime. CT value > 30 is regarded as non-specificity threshold. **C** Representative H&E-stained tissue sections from distal ileum, caecum, and proximal colon of *Tnf* $^{\Delta ARE}$ mice showing no (NR), low (LR), and high grade (R) of inflammation in the ileum as described above. **D** Analysis of bacterial localization in distal ileum of inflamed (R) and non-inflamed (NR) *Tnf* $^{\Delta ARE}$ mice from F1 generation by performing FISH staining with eubacterial 16S probe (red) and DAPI for nuclear visualization. **E** Quantitative analysis of *Tnf* and *Il-17A* mRNA expression in distal ileum of non-inflamed (NR) and inflamed (R *Tnf* $^{\Delta ARE}$ mice and WT controls. **F** Correlation analysis between Ileitis score and SFB abundance in intestinal contents and fecal pellets in the full cohort of 18-week-old *Tnf* $^{\Delta ARE}$ mice and **G** in 12 10-week-old (mild ileitis) and 12 > 24-week-old (severe ileitis) SAMP1/YitFc mice, respectively. We replaced all data points below the detection limit (threshold of Ct > 30) by a fixed minimal value Ct = 30 in (**F**, **G**). This illustrates the dataset more clearly than excluding the values under the detection limit completely from the analysis. Statistical significance was assessed by One-way-ANOVA followed by Tukey multiple comparison test. *$p < 0.05$; **$p < 0.01$; ***$p < 0.001$ was considered statistically significant

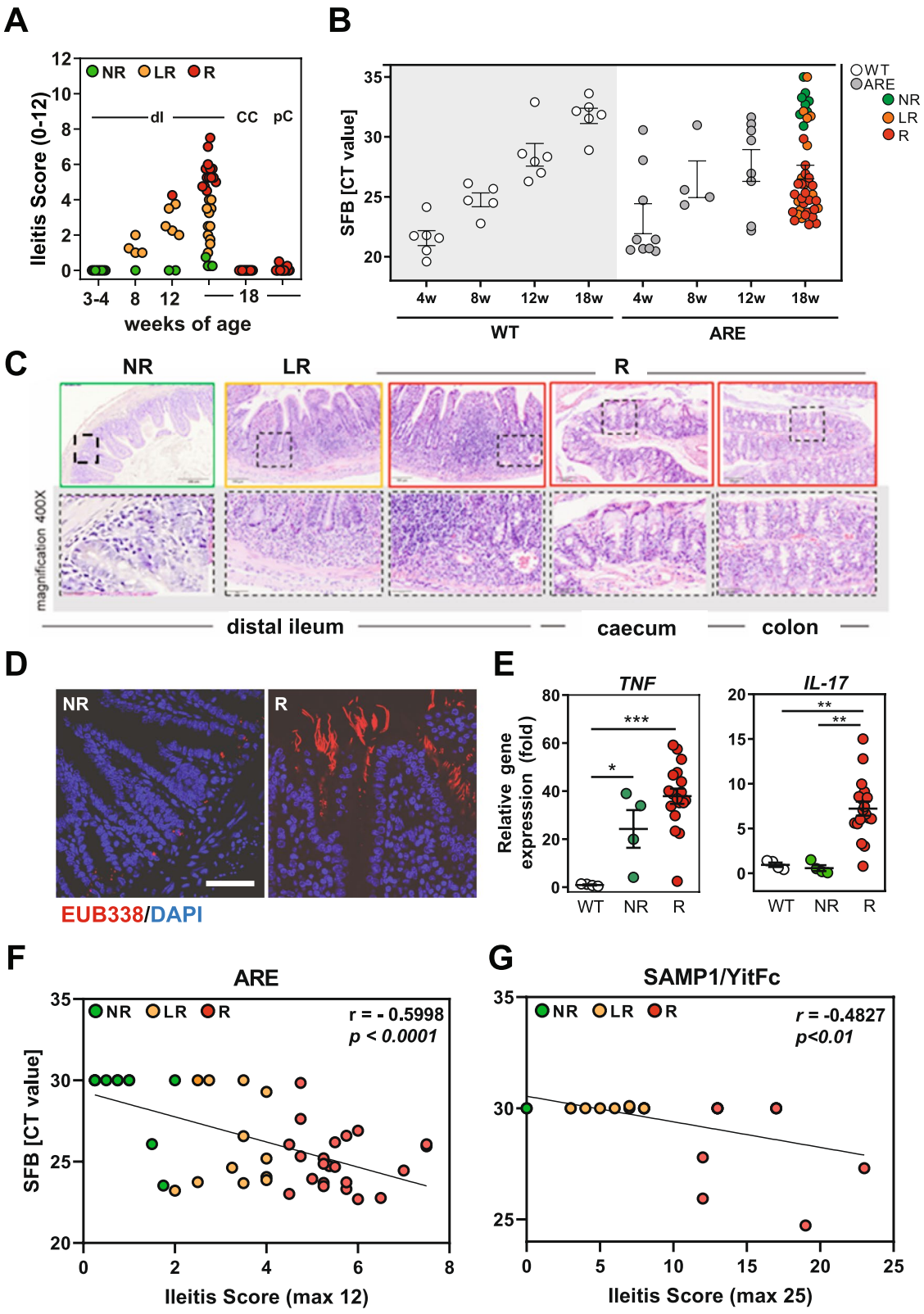

Fig. 1 (See legend on previous page.)

35, data not shown) in both monoassociated mice and mice colonized with the minimal bacterial consortium.

SFB promote intestinal inflammation in Tnf $^{\Delta ARE}$ mice

Next, we sought to investigate SFB-mediated immune modulation following high SFB exposure from birth. Therefore, GF WT mothers were monocolonized with SFB and mated with GF *Tnf* $^{\Delta ARE}$ males. Following maternal SFB exposure, mono-colonized offspring were analyzed at 4 and 12 weeks of age. Interestingly, 12-week-old SFB-mono-colonized *Tnf* $^{\Delta ARE}$ mice showed extensive ileo-colonic inflammation affecting small and large intestinal compartment, whereas 4-week-old mice remained completely disease-free (Fig. 2A). Comparable SFB abundance was detected in intestinal contents collected from ileal, colonic, and cecal compartments of monocolonized *Tnf* $^{\Delta ARE}$ and WT mice (Fig. 2B). SFB was localized in close contact to the intestinal epithelium of the inflamed tissue regions, such as the distal ileum and proximal colon but did not penetrate the mucus layer of the distal colon (Fig. 2C). Histopathological evaluation showed exacerbated inflammation in the ileum, cecum, and proximal colon, and no inflammation in the duodenum, jejunum, and distal colon (Fig. 2D). SFB are well known to specifically induce Th17 responses in mice under physiological conditions [32]. In SFB monocolonized mice, analysis of the inflammatory transcript levels revealed highly enhanced expression of *Tnf*, *Il-17A*, and *Ifng* in most of the affected mucosal tissue of 12-week-old *Tnf* $^{\Delta ARE}$ mice when compared to WT controls, while *Tnf* was only found to be significantly elevated in the distal ileum of 4-week-old *Tnf* $^{\Delta ARE}$ mice (Fig. 2E and Supplementary Figure S2A). Tissue pathology of inflamed *Tnf* $^{\Delta ARE}$ mice is characterized by a significantly increased immune cell infiltration, showing an increased number of IL-17-expressing cells in the tissue when compared to WT controls (Supplementary Figure S2B). However, the proportion of *Il-17*-expressing T cells remained unchanged between *Tnf* $^{\Delta ARE}$ mice and WT controls upon SFB colonization (Supplementary Figure S2C). In contrast, considerable changes in cell proportions were observed for *Ifng*-expressing T cells, but also neutrophilic granulocytes, which were both found to be highly enhanced in 12-week-old *Tnf* $^{\Delta ARE}$ mice (Supplementary Figure S2D, E, F,G). Next, we determined the expression of genes involved in antimicrobial defense at the epithelium in the distal ileum to investigate the signaling molecules that are produced by the host upon SFB colonization in 4-week and 12-week-old *Tnf* $^{\Delta ARE}$ mice. Twelve-week-old SFB mono-colonized *Tnf* $^{\Delta ARE}$ mice showed significantly reduced levels of antimicrobial peptides including Cryptdin 5 (Defensin a5) and lysozyme, two important types of intestinal antimicrobial peptides produced by Paneth cells in addition to Angiogenin 4 and C-type lectin regenerating islet-derived 3 beta (Reg3b) compared to WT controls .These findings suggest that dysregulation of antimicrobial peptides expression is a feature of homeostasis disruption in the inflamed intestine (Fig. 2F), revealing dysregulated antimicrobial defense response of the intestinal epithelium. Consistent with these findings, significantly reduced numbers of lysozyme-positive Paneth cells, as well as mucin-filled goblet cells were shown in inflamed 12-week-old *Tnf* $^{\Delta ARE}$ mice (Fig. 2G, H and Supplementary Figure S2H, I).

To further investigate the potential of elevated numbers of *IL-17*-expressing cells in activating inflammatory responses in *Tnf* $^{\Delta ARE}$ mice, we next analyzed the outcome of monocolonization with *Bifidobacterium adolescentis*, another human commensal bacterial strain that was recently reported to strongly induce Th17 cells in the murine intestine, particularly the ileal compartment [59]. *Bifidobacterium adolescentis* (strain L2-32) was introduced into 8-week-old GF *Tnf* $^{\Delta ARE}$ mice and littermate wild-type controls and housed in isolators for

(See figure on next page.)

Fig. 2 SFB mono-colonization causes CD-like inflammation in *Tnf* $^{\Delta ARE}$ mice. Germ-free *Tnf* $^{\Delta ARE}$ mice and littermate WT controls were monocolonized with SFB from birth. **A** Severity of inflammation was assessed by evaluating the tissue pathology score in tissue sections of distal ileum, cecum, and proximal and distal colon from 12-week-old WT mice as well as 4-week-old and 12-week-old *Tnf* $^{\Delta ARE}$ mice. **B** Quantitative analysis of SFB abundance in intestinal contents from distal ileum, cecum, and proximal and distal colon of 12-week-old WT and *Tnf* $^{\Delta ARE}$ mice. **C** FISH by using the eubacterial probe EUB338 was performed on tissue sections from distal ileum and colon of 12-week-old *Tnf* $^{\Delta ARE}$ mice followed by immunostaining with E-Cadherin. DAPI was used for nuclear visualization. Dotted line indicates thickness of inner mucus layer. **D** H&E-stained tissue sections of 12-week-old *Tnf* $^{\Delta ARE}$ mice revealed profound intestinal inflammation in the compartments of distal ileum, cecum, proximal colon, but not jejunum and distal colon when compared to 12-week-old WT controls, but also 4-week-old *Tnf* $^{\Delta ARE}$ mice. Scale bar represents 200 or 100 µm as indicated. **E** Quantitative analysis of *Tnf* and *Il-17A* transcript levels in mucosal tissue of distal ileum, cecum, and proximal colon from 4 and 12-week-old *Tnf* $^{\Delta ARE}$ mice and 12-week-old WT controls. Statistical significance was assessed by One-way analysis of variance (ANOVA) followed by Tukey test. *$p < 0.05$; **$p < 0.01$; ***$p < 0.001$ was considered statistically significant. **F** Quantitative analysis of *Muc2*, *Defa5*, *Ang4*, and *Reg3b* transcript levels in mucosal tissue of distal ileum from 4- and 12-week-old *Tnf* $^{\Delta ARE}$ mice and 12-week-old WT controls. Statistical significance was assessed by One-way analysis of variance (ANOVA) followed by Tukey test. *$p < 0.05$; **$p < 0.01$; ***$p < 0.001$ was considered statistically significant. **G** Immunofluorescence (IF) co-staining of Lysozyme (red) and E-cadherin (IEC borders, blue) counterstained with Dapi (nuclei, cyan) in ileal tissue sections from 4 weeks and 12 weeks mono-colonized WT and *Tnf* $^{\Delta ARE}$ mice (× 600) lower panel: higher magnification of the indicated sections (× 3600). **H** Quantification of the total number of Lysozyme positive Paneth cells per crypt based on IF staining. Statistical analyses were performed by one-way analysis of variance (ANOVA) followed by Tukey test

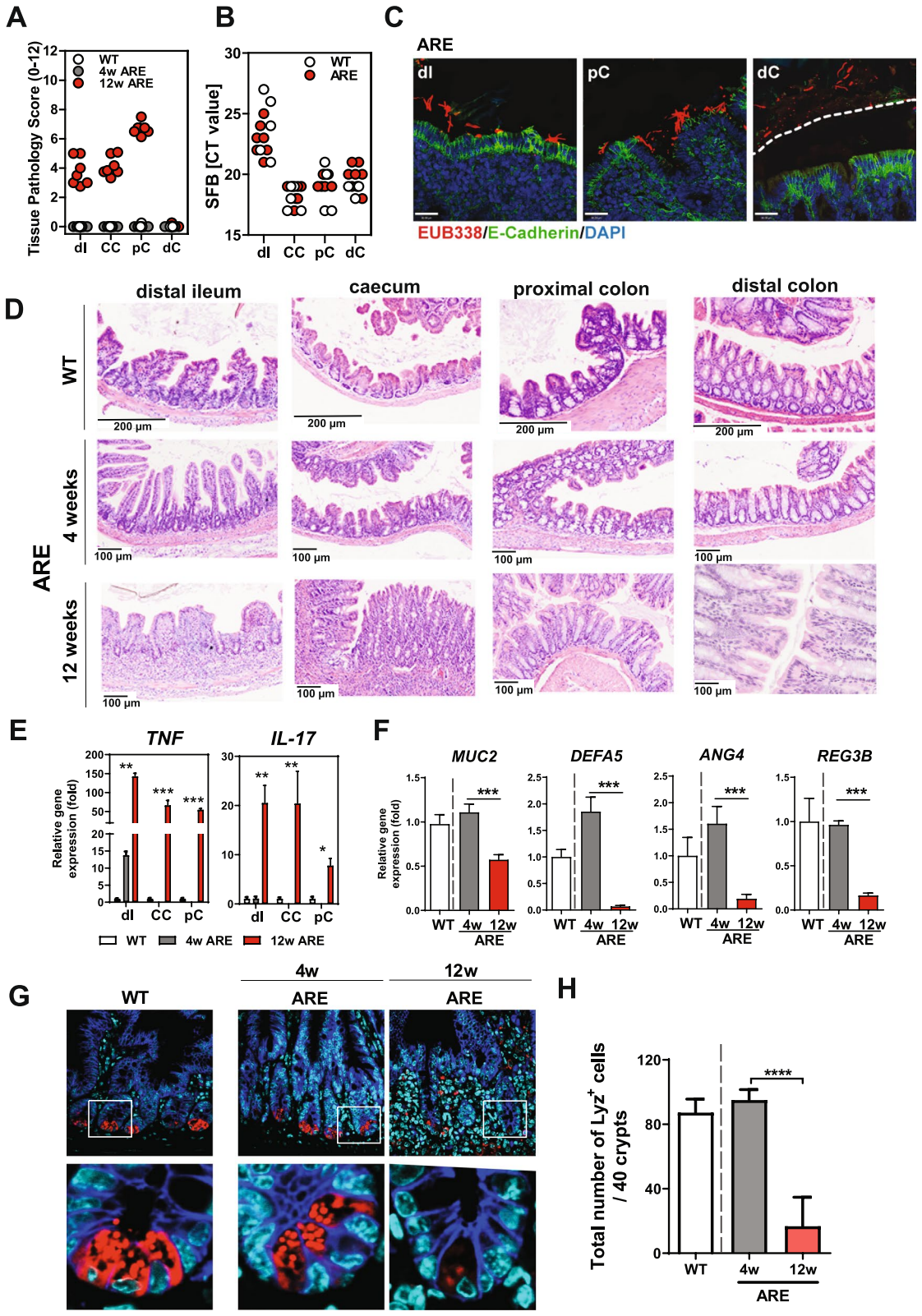

Fig. 2 (See legend on previous page.)

4 weeks before analysis (Extended Supplementary Figure S2A). Even though *B. adolescentis* has been strongly assumed to be pathologically involved in the aggravation of autoimmune arthritis, monocolonization did not trigger intestinal inflammation in *Tnf* $^{\Delta ARE}$ mice (Extended Supplementary Figure S2B, C). In contrast to SFB colonization in *Tnf* $^{\Delta ARE}$ mice, *B.adolescentis* only showed mild induction of TNF, but no differences in Il-17A or IFNg gene expression compared to their WT controls (Extended Supplementary Figure S2D). Accordingly, the numbers of lysozyme-positive Paneth cells in the distal ileum of *Tnf* $^{\Delta ARE}$ mice compared to WT mice remained unchanged (Extended Supplementary Figure S2E). Taken together, these findings indicate that the SFB-mediated pathology in *Tnf* $^{\Delta ARE}$ mice is highly associated with Th1-related immune responses, while general symbiont-driven IL-17 induction seems not to be sufficient to trigger intestinal inflammation in these mice.

SFB fail to induce ileo-colonic inflammation in a colitis mouse model

We clearly demonstrated that SFB induces ileo-colonic inflammation in mono-colonized *Tnf* $^{\Delta ARE}$ mice. As SFB are known to attach to intestinal epithelial cells and potently stimulate host immune response, we next wanted to test host specificity to the mucosal-adherent SFB. For this purpose, we assessed the impact of SFB colonization on colitis development in IL10-deficient *(Il10*$^{-/-}$129Sv) mice, known to develop Th1/Th17-related and microbiota-dependent colonic inflammation. In addition, we mono-colonized age matched *Tnf* $^{\Delta ARE}$ mice and WT controls for the same time frame. All groups were colonized at 8 weeks of age and analyzed 4 weeks later (Fig. 3A). Intriguingly, SFB colonization did not induce inflammation in any of the intestinal compartments of *Il10*$^{-/-}$ mice. In contrast, *Tnf* $^{\Delta ARE}$ mice showed exacerbated inflammation in the proximal colon and in cecum tissue, and expectedly in the distal ileum tissue (Fig. 3B), as shown by microscopic analysis of H&E-stained tissue sections (Fig. 3D). The presence of SFB in *Il10*$^{-/-}$ as well as *Tnf* $^{\Delta ARE}$ mice and their matching WT controls was confirmed using SFB-specific qPCR assay. Comparable SFB loads were observed in intestinal contents collected from ileal, colonic, and cecal compartments of both mouse models (Fig. 3C). To specifically examine changes in colon tissue morphology in both mouse models, we performed PAS/AB goblet cell staining in proximal colon tissue. The results showed significantly reduced numbers of PAS/AB positive mucin filled goblet cells in inflamed *Tnf* $^{\Delta ARE}$ mice, while *Il10*$^{-/-}$ mice remained unaffected (Fig. 3E, F).

Detection of segmented filamentous bacteria in tissue biopsies of patients with inflammatory bowel diseases

The presence of SFB in the intestine of various species, including rodents, pigs, chicken, and fish have been previously reported [60]; however, findings describing the presence of SFB in human gut are rather limited. To investigate the prevalence of SFB in IBD patients, we next sought to examine the presence of SFB in human mucosal biopsies and screened 468 ileal and colonic biopsies derived from 3 independent cohorts of IBD patients (Fig. 4A). We used a PCR approach and the primers previously published by Jonsson [29] and by Snel [54] and the newly designed primer set (unpublished data, Pamela Schnupf). In addition, we used SFB cloned DNA and 2 SFB human biopsies positive for SFB as positive control. In these experiments, 0.3 or 3 ng of input DNA was used, and gene amplification of the newly designed primer set was confirmed by the detection of the expected 200 bp PCR product via gel electrophoresis (Fig. 4C). While only 27/412 samples showed CT values below 35 using the previously published primer set (PS01), PCR yielded random amplification with SFB identity not verified. The second and newly designed primer set (PS02) showed specific amplification and the identity of amplified PCR products with SFB was verified by DNA sequencing and alignment to the positive control (Fig. 4B, Extended Supplementary Figure S3A–D). Nevertheless, none of the analyzed tissue biopsies (0/468), including those that proved to be positive using the first primer-set showed to be positive for SFB.

We recently reported that the transplantation of fecal microbiota from CD patients successfully recreated the disease phenotype in recipient *Il10*$^{-/-}$ GF mice, while WT mice remained disease-free. Changes in immune cell profiles mirrored the level of tissue pathology and

(See figure on next page.)

Fig. 3 SFB fail to induce ileo-colonic inflammation in a colitis mouse model. **A** GF *Tnf* $^{\Delta ARE}$, *Il10*$^{-/-}$ mice and WT controls were mono-colonized with SFB from 8 to 12 weeks of age. **B** Severity of inflammation was assessed by evaluating the tissue pathology score in tissue sections of cecum, proximal, and distal colon from *Tnf* $^{\Delta ARE}$ mice and *Il10*$^{-/-}$ mice, respectively. **C** Quantitative analysis of SFB abundance in intestinal contents collected from ileal, colonic, and cecal compartments of 12-weeks-old *Tnf* $^{\Delta ARE}$ mice and *Il10*$^{-/-}$ mice, respectively. **D** H&E-stained tissue sections of *Tnf* $^{\Delta ARE}$ mice revealed intestinal inflammation in the compartments of distal ileum, cecum, proximal colon, compared to *Il10*$^{-/-}$ mice. Scale bar represents 200 or 100 µm as indicated. **E, F** PAS-AB goblet cell staining in proximal colon tissue sections from mono-colonized *Tnf* $^{\Delta ARE}$ and *Il10*$^{-/-}$mice (× 400). Lower panel represents higher magnification (× 1200) of the indicated sections. Graph represents the quantification of goblet cells per crypt. Statistical analyses were performed by unpaired Student's *t* test

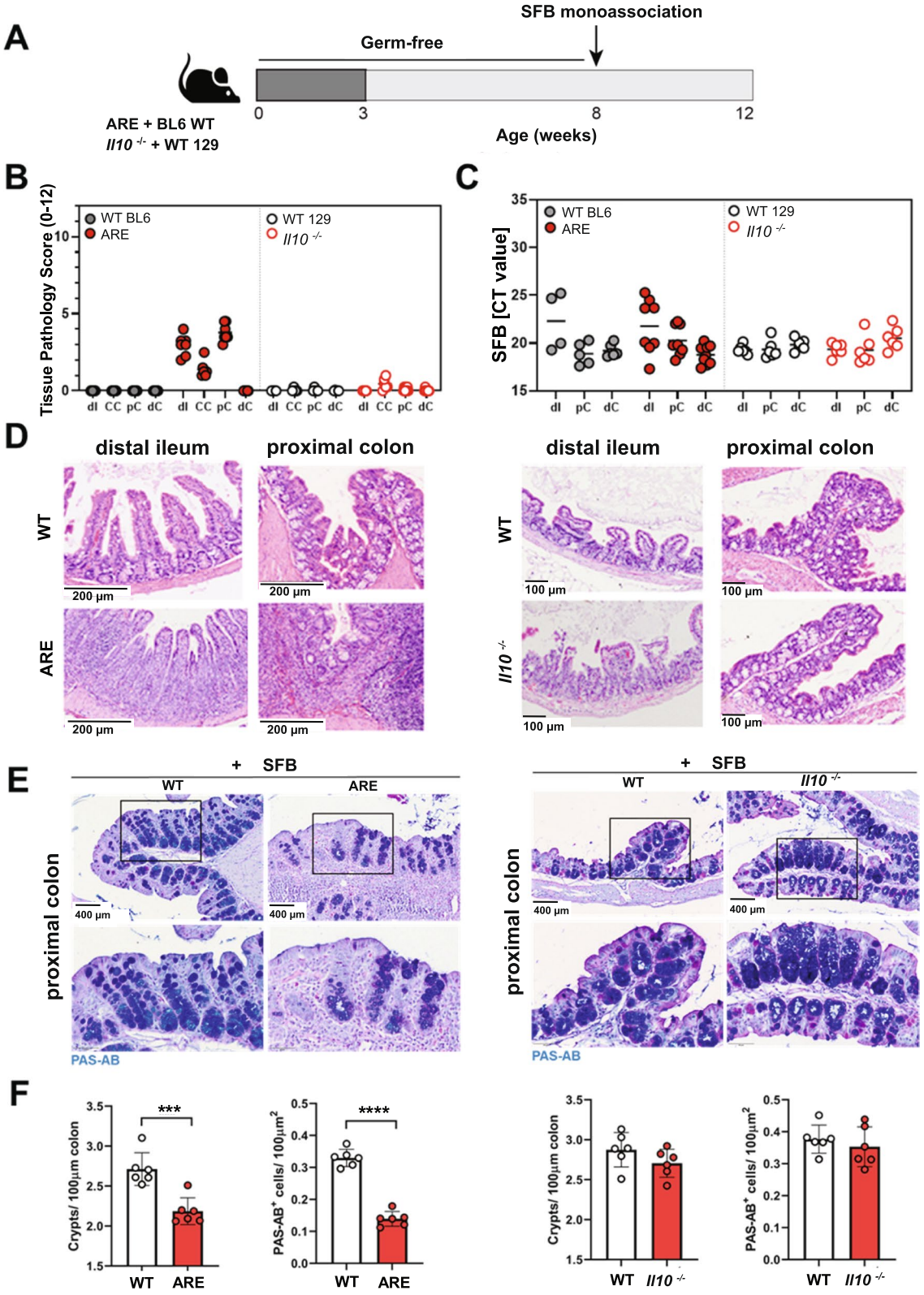

Fig. 3 (See legend on previous page.)

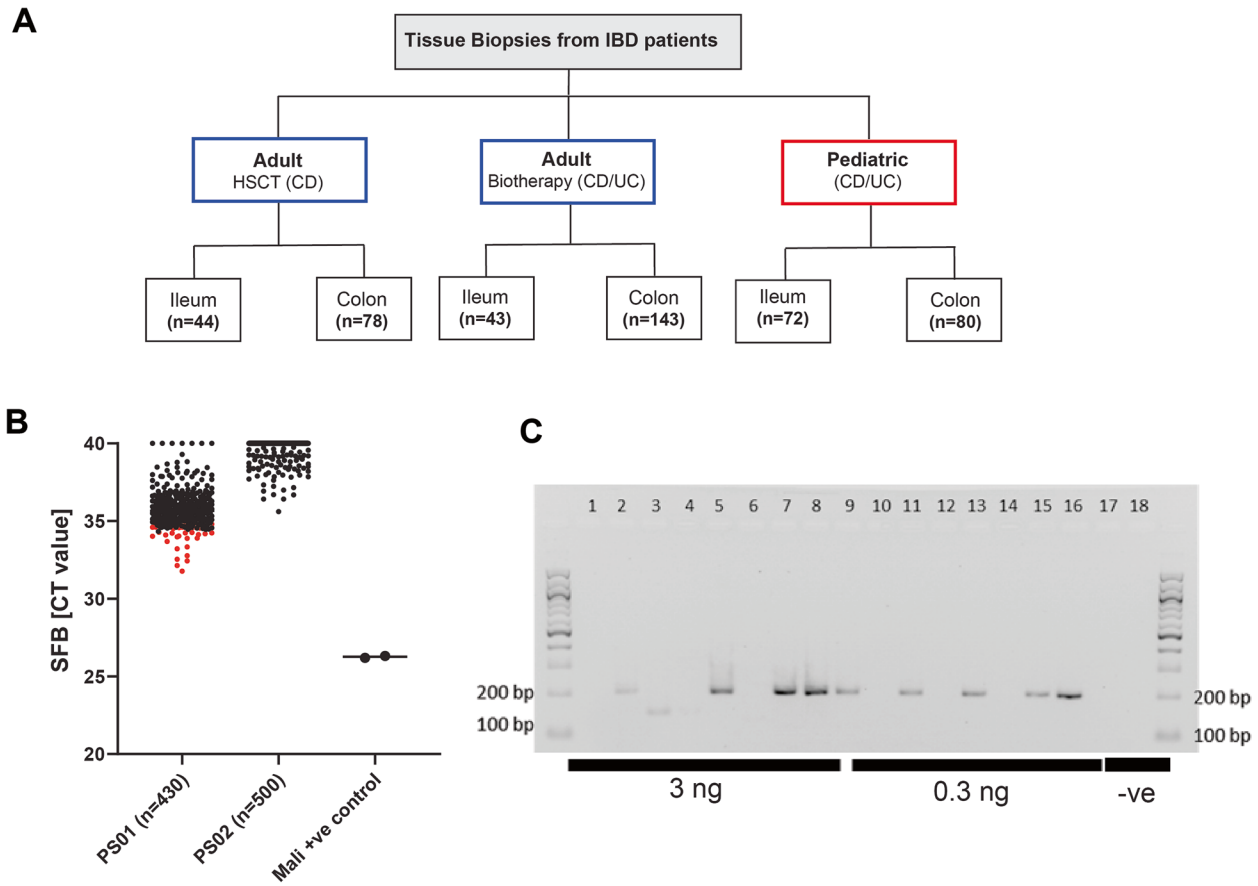

Fig. 4 PCR detection of segmented filamentous bacteria in tissue biopsies of patients with Inflammatory bowel diseases. **A** Human cohorts screened for the presence of SFB.The analyzed samples included mucosal biopsies collected from three IBD patient cohorts enrolled in Barcelona, Paris and Munich. The Spanish (HSCT) cohort included patients enrolled in follow-up for CD following treatment with autologous hematopoietic stem cell transplantation (AHSCT). Ileal (n=44) and colonic biopsies (n=86) from CD patients were included in the analysis. The French (Biotherapy) cohort included longitudinally collected samples from CD and UC patients who are treated with anti-TNF and other biotherapy drugs and recruited in Paris. Ileal (n=43) and colonic biopsies (n=143) from CD and UC patients were included in the analysis. The German pediatric cohort is a longitudinal prospective study comprising children with IBD and were recruited in Munich. Ileal (n=72) and colonic biopsies (n=80) were included in the analysis. A positive control of DNA extracted from a sample positive for SFB positive based on 16S sequencing (Mali, provided by Pamela Schnupf) **B** Quantitative analysis of SFB abundance in tissue biopsies using two primer sets (published by Jonsson [29] and by Snel [54] and the newly designed primer set; unpublished data, Pamela Schnupf). Quantification of SFB in human tissue biopsies was performed using the MasterMix SensiFAST™ SYBR (BIOLINE) and 3 different primer sets: for_5'-TGTGGGTTGTGAATAGCAAT-3', rev_5'-GCGAGCTTCCCTCATTACAAGG-3', for_5'-AGG AGGAGTCTGCGGCACATTAGC-3' ,rev_5' TCCCCACTGCTGCCTCCCGTAG-3' and for,_ 5'-TGTAGGTTGTGAAGAACAAT-3', rev_ 5'-GCGAGCTTCCCTCAT TACAAGG-3' (modified primer sequences, unpublished data, Pamela Schnupf). **D** Gel electrophoresis showing expected 200 bP PCR products in a selected subset of samples and no bands in the negative control.

confirmed the transmissibility of disease activity in gnotobiotic mice [15]. Here, we transplanted fecal microbiota from CD patients at baseline (active disease) or during remission (inactive disease) into GF *Tnf* $^{\Delta ARE}$ mice. Mice were colonized at 8 weeks of age and assessed for tissue pathology at 12 weeks of age. Nevertheless, and despite the pathogenic potential of human CD-relevant microbial communities at baseline, the fecal microbiota transfer failed to induce inflammation in GF TNF$^{\Delta ARE}$ mice. Interestingly, SFB were absent in mucosal biopsies derived from both patients at the same timepoints (Ct-value = 40). Moving forward, we wanted to test the capability of SFB to drive a remission-associated complex microbial community towards inflammation. To this end, we transplanted CD patient microbiota alone and in co-colonization with SFB into GF *Tnf* $^{\Delta ARE}$ mice. We colonized two groups of *Tnf* $^{\Delta ARE}$ mice and WT controls, either with fecal microbiota from CD patient only or in combination with SFB. Both groups were colonized at 8 weeks of age and assessed for tissue pathology at 12 weeks of age (Supplementary Figure S3A). Since SFB pathogenicity is seemingly dependent on the microbial

community context besides the genetic susceptibility of the host, we wanted to test the capability of SFB to reactivate the pathogenic potential of a complex microbial community derived from CD patient. Consistent with our previous finding in *Il10*$^{-/-}$ [15], CD human remission microbiota transfer into *Tnf* $^{\Delta ARE}$ mice did not show any signs of inflammation or changes in ileal histopathology 4 weeks after colonization. However, SFB co-colonization induced inflammation in humanized *Tnf* $^{\Delta ARE}$ mice in contrast to mice colonized only with CD human microbiota (Supplementary Figure S3B, D). SFB quantification using qPCR assay confirmed the colonization of SFB in intestinal contents collected from ileal, colonic, and cecal compartments of the co-colonized mice (Ct values = 25.1 ± 2.4), while they were undetectable (Ct values ≥ 35) in mice colonized only with human CD microbiota (Supplementary Figure S3C). Consistently, SFB co-colonization resulted in reduced numbers of Lysozyme positive Paneth cells (Supplementary Figure S3E, F). To characterize microbial community shifts driven by the co-colonization with SFB, microbiota profiling of gut content showed a clear separation between *Tnf* $^{\Delta ARE}$ mice colonized with CD human microbiota alone or in combination with SFB. These changes were characterized by an overabundance of *Alistipes* and *Bilophila* (Supplementary Figure S3G, H). Interestingly and like the microbial shifts observed in humanized SFB co-colonized mice, *Alistipes* showed to be one of the most significantly differential taxa in *Tnf* $^{\Delta ARE}$ mice under SPF conditions.

EEN-like purified diet eradicates SFB and prevents CD-like ileo-colonic inflammation in Tnf $^{\Delta ARE}$ mice

To simulate the protective effect of exclusive enteral nutrition (EEN) therapy in humans, we fed *Tnf* $^{\Delta ARE}$ mice and WT matching control EEN-like purified diet (PD) directly after weaning and characterized bacterial and host responses after 10 weeks of feeding. Our data showed that PD completely inhibited the development of intestinal inflammation in *Tnf* $^{\Delta ARE}$ mice (Supplementary Figure S4A). The diet-mediated protection was also associated with substantial changes in community structure (Supplementary Figure S4C). Interestingly, SFBs were not detected in the intestinal microbiota of PD-treated *Tnf* $^{\Delta ARE}$ mice (Supplementary Figure S4B).

To investigate the direct influence of diet on SFB colonization and on intestinal inflammation, we performed four SFB monocolonization experiments using three differet diets, including chow diet, PD control diet and purified fiber-rich diet (FRD) (Fig. 5A). In the first experiment, WT and *Tnf* $^{\Delta ARE}$ mice were colonized with SFB at 8 weeks of age and were fed with chow diet until the end of the experiment. In the second and third experiments, the mice were colonized with SFB at 8 weeks of age and were exposed to purified PD 1 week before or after SFB colonization (7 weeks or 9 weeks of age, respectively). In the fourth experiment, the mice were exposed to FRD 1 week before SFB colonization. Expectedly, SFB quantification using qPCR assay confirmed the presence of SFB in ileal, cecal, and colonic content of both WT and *Tnf* $^{\Delta ARE}$ SFB monocolonized mice fed with chow diet (Ct values = 21.5 ± 2.5). On the other hand, SFB were undetectable (Ct values ≥ 35) in intestinal contents collected from ileal, colonic, and cecal compartments of SFB-monocolonized mice fed with PD before or after SFB colonization. Interestingly, the re-introduction of fiber using FRD allowed the partial colonization of SFB in WT and *Tnf* $^{\Delta ARE}$ mice (Ct values = 32.4.5 ± 3.5) (Fig. 5B). Histopathological evaluation revealed inflammation in the distal ileum and proximal colon of *Tnf* $^{\Delta ARE}$ mice fed with chow diet, while mice fed with PD or FRD showed no signs of inflammation (Fig. 5C). Consistently, a significantly reduced number of lysozyme positive Paneth cells was observed in *Tnf* $^{\Delta ARE}$ mice on chow diet compared to mice on PD, while mice on FRD showed intermediate levels of lysozyme positive Paneth cells (Fig. 5D, E). Gene expression analysis on tissue sections from distal ileum showed significantly elevated expression of *Tnf* and *Il-17A* in *Tnf* $^{\Delta ARE}$ mice mono-colonized with SFB and fed with chow diet compared to those fed with PD or FRD (Fig. 5F). To visualize SFB in tissue sections of *Tnf* $^{\Delta ARE}$ mice under different dietary conditions, we performed fluorescence in situ hybridization (FISH) by staining proximal colon sections with bacteria domain-specific (EUB338) probes. Microscopic examination showed growth of filamentous bacteria close to the intestinal

(See figure on next page.)

Fig. 5 EEN-like PD eradicates SFB and prevents CD-like ileo-colonic inflammation in *Tnf* $^{\Delta ARE}$ mice. **A** Germ-free *Tnf* $^{\Delta ARE}$ mice and littermate WT controls were mono-colonized with SFB at 8 weeks of age and exposed to chow, EEN-like PD or fiber-rich PD. **B** Quantitative analysis of SFB abundance in ileal, cecal, and colonic contents of chow-fed, PD-fed or FRD-fed WT and *Tnf* $^{\Delta ARE}$ mice. **C** Severity of inflammation was assessed by evaluating the tissue pathology score in tissue sections of distal ileum, proximal, and distal colon in WT and *Tnf* $^{\Delta ARE}$ mice. **D** Immunofluorescence (IF) co-staining and quantification of Lysozyme (red) and E-cadherin (IEC borders, blue) counterstained with Dapi (nuclei, cyan) in ileal tissue sections from mono-colonized and chow, PD-fed or FRD-fed WT and *Tnf* $^{\Delta ARE}$ mice (600x) lower panel: higher magnification of the indicated sections (3600x). **E** Quantitative analysis of Tnf and Il-17A transcript levels in mucosal tissue of distal ileum from mono-colonized and chow, PD-fed or FRD-fed WT and *Tnf* $^{\Delta ARE}$ mice. **F** FISH by using the eubacterial probe EUB338 was performed on tissue sections from distal ileum and colon of chow-fed, PD-fed or FRD-fed WT and *Tnf* $^{\Delta ARE}$ mice followed by immunostaining with E-Cadherin. DAPI was used for nuclear visualization. Dotted line indicates thickness of inner mucus layer

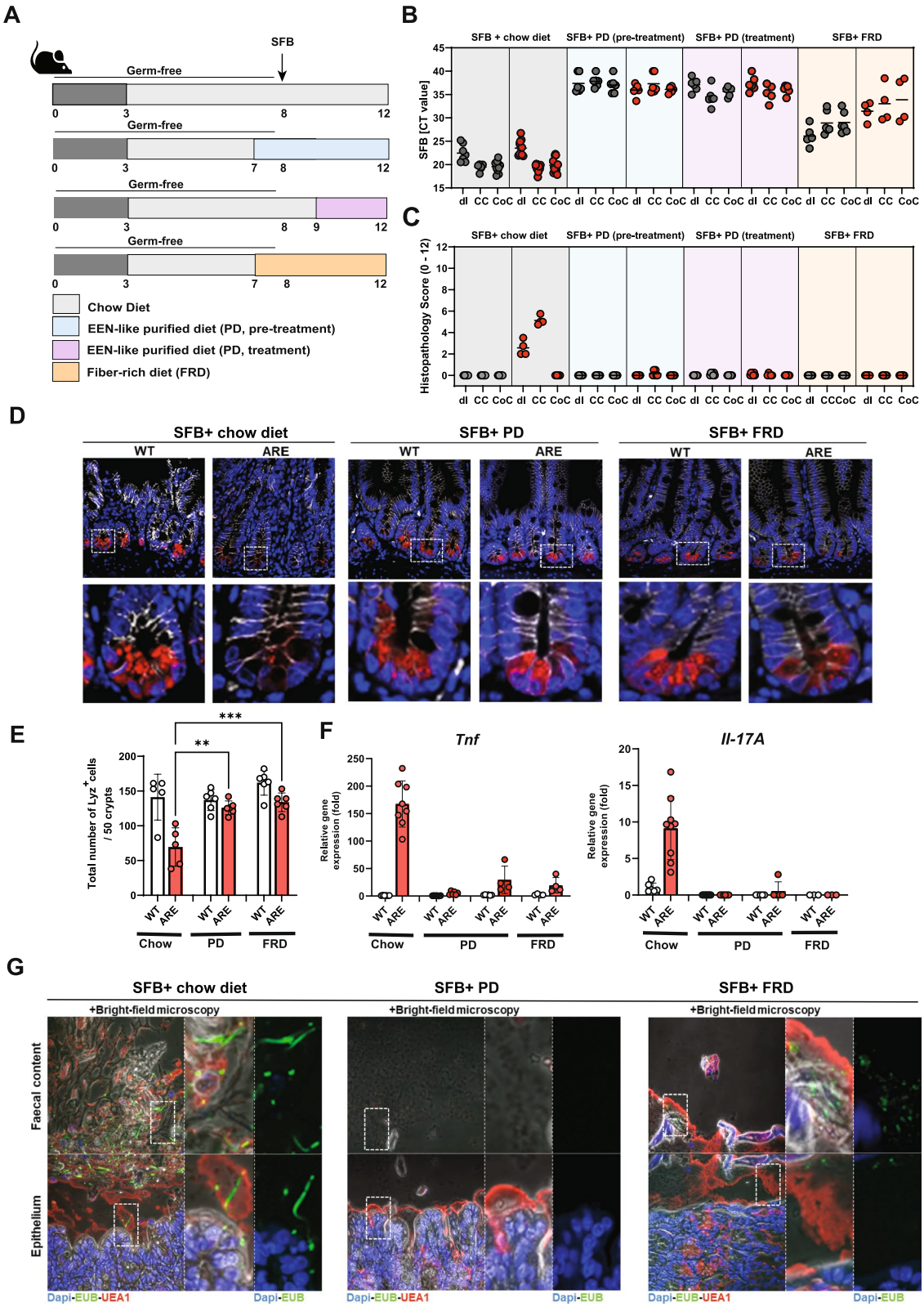

Fig. 5 (See legend on previous page.)

epithelium in *Tnf* $^{\Delta ARE}$ mice on chow diet and to lesser extent in *Tnf* $^{\Delta ARE}$ mice on FRD, while they were not visible in *Tnf* $^{\Delta ARE}$ mice under PD (Fig. 1G).

Discussion

Accumulating evidence suggests a crucial role of the intestinal microbiota in the onset and progression of inflammatory bowel diseases [61–63]. Previous reports identified a few pathogenic bacteria that are enriched in dysbiotic microbial communities and lead to disease development [64, 65]. In the present study, we aimed at identifying the causal microbial cues responsible for inducing or modulating Crohn's disease-like inflammation in *Tnf* $^{\Delta ARE}$ mice. Intriguingly, histological analysis of ileal tissue sections clearly revealed the detection of filamentous bacteria in inflamed responder mice, closely resembling the commensal SFB. SFB are well known to induce the maturation of Th17 cell-derived immune responses, which are highly implicated in the pathogenesis of IBD [66]. However, assessment of disease development kinetics in *Tnf* $^{\Delta ARE}$ mice showed that both *Tnf* $^{\Delta ARE}$ mice as well as littermate WT controls harbour significantly higher SFB loads at the age of 3–4 weeks, which declined below detectable levels in adult mice, under non-inflammatory conditions. Similar observations were reported, describing bacterial alterations as an ongoing physiological process in line with the intestinal mucus layer maturation upon bacterial colonization [67]. Interestingly, we showed that in adult *Tnf* $^{\Delta ARE}$ mice, the abundance of SFB strongly correlated with the severity of ileal inflammation, suggesting that SFB growth is driven by changes in the bacterial community composition, subsequently leading to inflammation.

We then investigated whether SFB can persist in a maturate immune system, and whether they are capable of driving changes in a complex intestinal bacterial community towards inflammation. Interestingly, the introduction of SFB in SPF-housed 8 weeks old *Tnf* $^{\Delta ARE}$ mice significantly enhanced the abundance of *Alistipes* species that has been previously reported to trigger colitis and tumor growth in *Il-10*-deficient mice [68]. Under physiological conditions, the growth of *Alistipes* is suggested to be regulated by iron availability [69]. In this context, work from our group showed that the induction of inflammation in *Tnf* $^{\Delta ARE}$ mice seemed to be highly dependent on the availability of dietary iron since mutant mice fed with low-iron diet remained healthy and showed no signs of inflammation [70]. Conclusively, we suggested that *Alistipes* might be involved in the onset of CD-like ileitis in *Tnf* $^{\Delta ARE}$ mice, but monocolonization of mice with *Alistipes* was not sufficient to trigger inflammation, unlike SFB which is also known to utilize iron as an energy source for growth [71]. We next proposed that most likely inflammation in *Tnf* $^{\Delta ARE}$ mice is triggered by the mere presence of SFB. Here we showed that the monocolonization of GF *Tnf* $^{\Delta ARE}$ mice with SFB from birth and for 12 weeks could induce severe inflammation which expanded to the colon, thereby demonstrating for the first time the potential pathogenic role of these commensal bacteria in the intestine independent of synergism with complex microbiota [72, 73]. In homeostatic conditions, SFB are well known to preferentially induce the differentiation of intestinal mucosal Th17 cells. However, SFB-monocolonized *Tnf* $^{\Delta ARE}$ mice revealed, in addition to highly upregulated gene expression of TNF, IL-17A, and IFNg, significantly expanded populations of IFN-expressing CD4+ cells in inflamed ileum, caecum and colon, whereas the proportion of IL-17A-expressing T cells was similar between inflamed *Tnf* $^{\Delta ARE}$ mice and their WT controls. Besides, we observed a small proportion of double positive Th17+IFNγ+ positive cells in lamina propria of inflamed SFB-monoassociated mice, but the Th1-like cell population was predominant. This was accompanied by expanded neutrophilic granulocytes and an impaired epithelial antimicrobial defense of the intestine. Generally, TNF is upregulated in *Tnf* $^{\Delta ARE}$ mice upon microbial colonization. Our findings suggest that the basally increased *Tnf* transcript levels are not sufficient to induce inflammation in *Tnf* $^{\Delta ARE}$ mice, but rather cause changes in the immune responses triggered by SFB. Here, we observed highly expanded populations of neutrophilic granulocytes driven by the pro-inflammatory cytokine milieu in the inflamed gut of SFB-monoassociated *Tnf* $^{\Delta ARE}$ mice. In this context, Flannigan et al. [74] described the recruitment of neutrophils into the ileum upon SFB-mediated IL-17A expression as a control mechanism limiting SFB expansion in the gut. The enhanced neutrophil infiltration in *Tnf* $^{\Delta ARE}$ mice seemed not to affect SFB growth in SPF-housed *Tnf* $^{\Delta ARE}$ mice but rather reflects an inefficient antimicrobial defense further associated with an impaired barrier function of the intestinal epithelium, which altogether might result in a Th1/Th17-driven inflammatory phenotype. One proposed mechanism contributing to IBD pathology lies in the ability of Th17 cells to transition into Th1 cells, rather than in Th17 cells alone [75], potentially explaining why therapy with anti-IL17A monoclonal antibodies was ineffective in CD patients [76].

The concept of pathogenic and non-pathogenic Th17 cells in the context of inflammatory diseases has previously been proposed [77, 78]. While the role of microbiota for the Th17 developmental plasticity in the intestinal immune response is of great importance, it is still unclear how to differentiate between pathogenic Th17 cells in response to pathogens and the non-pathogenic Th17 cells induced by commensals. Prior work showed that

SFB-induced resident intestinal Th17 were characterized by IL-22 and IL-17A expression and limited plasticity, whereas those elicited by epithelium-adhering pathogen *Citrobacter rodentium* switched towards Th1-like IFNγ production [79]. We demonstrated that SFB is able to induce alternative Th1-like cell response which in combination with profound infiltration of neutrophil granulocytes and impaired mucosal defense results in severe inflammation in small and large intestine. It remains important to decipher the contribution of specific immune cell subpopulations in SFB-triggered disease progression and their role in controlling SFB expansion. Thereby, neutralization experiments with anti-IFNg, IL17, and TNF antibodies would be a reasonable approach.

Consistent with these findings, high SFB loads have been reported in a subset of UC patients, suggesting a potential role for SFB in driving intestinal inflammation in human [30]. Nevertheless, it needs to be acknowledged that contradictory data exist regarding the presence of SFB in humans. An early report described the presence of a filamentous organism, potentially being SFB, on the ileal mucosa of a human subject using light microscopy [26]. In 2011, a large-scale study by Scyesnak et al. concluded that SFB are not present in humans based on metagenomic datasets search [71]. These findings were contradicted by a report showing the presence of SFB in human feces from many individuals. Arguably, the 16S rRNA gene sequences corresponding to human SFB in this work showed to cluster together with mouse SFB sequences [28]. In a recent work, Jonsson et al. published the draft genome sequence of human-adapted representative of SFB in a human ileostomy sample [53] which was validated by screening metagenomic datasets and identifying individuals carrying sequences identical to the new SFB genome. In the present study, we investigated the presence of SFB in 468 tissue biopsies collected from three independent cohorts of adult and paediatric IBD patients. We screened and analyzed the mucosal biopsies using previously published [30] and newly designed human SFB specific primers, based on the recently published SFB human genome sequence [53]. Interestingly, SFB were absent in ileal and colonic mucosal biopsies from IBD patients with active or inactive disease To test the capability of human gut microbiota to drive inflammation in *Tnf* $^{\Delta ARE}$ mice as we and others showed previously using *Il-10*-deficient mice [15, 80], we colonized *Tnf* $^{\Delta ARE}$ mice with fecal microbiota derived from an IBD patient. Surprisingly and in contrary to *Il-10*-deficient mice, the same patient microbial communities failed to induce inflammation in *Tnf* $^{\Delta ARE}$ mice. Considering the strong immunomodulatory functions of SFB, they can pose a synergistic effect with other commensal bacteria to drive beneficial or detrimental effects on the host physiology [60]. Investigating the capability of SFB to reactivate the pathogenic potential of human-derived microbiota through dual colonization of *Tnf* $^{\Delta ARE}$ with SFB and IBD patient-derived gut microbiota led to ileal inflammation together with reduced numbers of functional Paneth cells in *Tnf* $^{\Delta ARE}$ mice, suggesting that SFB contribute to microbial community and regulatory immune response modulation, leading to inflammation. Notably, the beneficial modulatory effect of SFB in a complex microbial community was shown in a recent study, where co-colonization with SFB abolished the murine norovirus (MNV)-induced colitis in Altered Schaedler Flora (ASF) colonized mice. In this context, SFB colonization enhanced the expression of pro-inflammatory cytokines and antimicrobial peptides, leading to inhibition of inflammation [81].

Intriguingly, prior evidence showed that dietary composition is an important determinant of the presence of SFB in the mouse small intestine. In an early study, the exclusive feeding in mice with milk powder showed to inhibit the growth and colonization of SFB when compared to complete laboratory mouse diets feeding [39]. In this study, the authors used twenty-one different purified diets as mouse feed to identify the macronutrients that might be responsible for SFB growth and colonization. Interestingly, none of the purified diets allowed SFB growth; however, the critical dietary cues responsible for these observations were not identified [39]. These findings suggest an important role of diet in modulating SFB growth and hence SFB-mediated inflammation.

The best and most prominent evidence for the ability of specific nutritional intervention in IBD treatment stems from the use of exclusive enteral nutrition (EEN) as induction therapy for pediatric CD. Changes in microbiota composition upon EEN therapy have been recently demonstrated [82], but the causality behind the success of this dietary intervention is not understood. EEN is a therapeutic nutrition confined in most cases to liquid fiber-free enteral formulas of typically synthetic or semi-synthetic composition. Here, we showed that consistent with the impact of EEN on disease activity in pediatric CD patients, the use of a purified experimental diet that is low in fiber content completely inhibited the development of CD-like ileitis in *Tnf* $^{\Delta ARE}$ mice under SPF housing conditions. These effects were associated with substantial changes in community structure. To elucidate the direct effect of the purified diet on SFB growth and mediated inflammation, we performed mono-colonization studies and showed that the pre-treatment or subsequent treatment of SFB mono-colonized *Tnf* $^{\Delta ARE}$ mice with the EEN-like purified diet completely prevented or abolished SFB, respectively. One of the main differences

between PD or EEN and chow diet is the presence of dietary fibers. Interestingly, in a previously published dietary intervention study, SFB were detected in two ileostomy samples from one patient during high-fiber diet intake, while they were not present in samples from the same patient during low-fiber diet intake. Consistently, data from clinical trials showed that the clinical efficacy of EEN in children with CD is rapidly lost after return to habitual diet, suggesting that the reintroduction of certain dietary components triggers the recurrence of intestinal inflammation. Further, in a previously published pilot study on 14 EEN-treated CD pediatric patients, a potential role of dietary fibers in inflammation recurrence after early re-introduction of solid food post-EEN was shown [83]. Based on the observations that SFB are present at higher abundances during weaning in many animals which could be because of the introduction of solid food or dietary fiber instead of mother's milk, we hypothesized that fiber could be a critical determinant of SFB propagation in *Tnf* $^{\Delta ARE}$ mice. Parallel to these findings, an early study in 1992 demonstrated that fibre-rich beans lead to an increased SFB colonisation in mice, when added to a natural diet [84]. Generally, fibers have been considered beneficial for gut health and several lines of evidence supported the importance of dietary fibers and their fermentation products in maintaining intestinal homeostasis and gut health in the context of IBD. For example, a clinical study by Brotherton et al. [85], including a 26-item dietary survey collected from 1130 CD and 489 UC patients, concluded that higher fiber consumption was associated with 40% lower probability of disease flare at 6 months among participants with CD. No significant association has been found in the case of patients with UC [85]. These findings suggested that dietary fiber deprivation is associated with greater risk of CD recurrence in a 6-month period. Consistently, findings from dietary fiber deprivation in humanized mice resulted in increased consumption of colonic mucosa by resident microbes leading to colonic inflammation [86] and data from additional clinical trials showed that short-chain fatty acids play a key role in the prevention of intestinal atrophy in IBD patients, resulting in tissue recovery [87]. Further and in a recent work investigating the specific contributions of dietary fiber and mucin-degrading intestinal microbiota to the development of inflammation in *Il10*-deficient mice, low dietary fiber promoted bacterial erosion of the protective colonic mucus layer by mucin-degrading bacteria, resulting in lethal colitis mediated by Th1immune response, expansion of natural killer T cells and reduced levels of IgA-coated bacterial species [88]. Nevertheless, recent studies highlighted the complexity of fiber composition and the importance of investigating the specific role of different fiber subtypes, including soluble and insoluble fibers representing varying chemical structures and fermentation output. For instance, Armstrong et al. addressed the role of microbiota and fiber fermentation processes in patients with IBD and reported that a subset of fibers, the unfermented dietary β-fructan fibers could induce proinflammatory cytokines in a subset of patients with IBD via activation of the NLRP3 and TLR2 pathways; suggesting that dietary fibers could have detrimental effects in selected patients with active IBD and who specifically lack microbes with fiber-fermentation capabilities [89].

In conclusion, this study aimed to identify the causal microbial cues responsible for CD-like inflammation and to dissect the protective role of diet in gnotobiotic mouse models providing a causal link between pathobiont expansion and CD-like ileo-colonic inflammation. We identified a novel pathogenic role of SFB in driving severe ileo-colonic inflammation in murine models, while SFB was undetectable in mucosal biopsies from IBD patients. Simulating the protective effect of EEN by feeding SFB mono-associated *Tnf* $^{\Delta ARE}$ mice chow diet or EEN-like purified diet showed that the pre-treatment or the subsequent treatment of SFB mono-colonized *Tnf* $^{\Delta ARE}$ mice with EEN-like purified diet prevented SFB colonization and completely abolished SFB-mediated inflammation, suggesting that fiber maybe an important determinant of pathobiont expansion and ileal inflammation in this model, proposing a plausible mechanism explaining the effectiveness of exclusive enteral nutrition in treating children with CD.

Supplementary Information

The online version contains supplementary material available at https://doi.org/10.1186/s40168-023-01508-y.

Additional file 1: Supplementary Figure S1. SFB abundance correlates with ileitis severity in SPF-house *Tnf* $^{\Delta ARE}$ (A) SPF-housed 8-week-old ARE and WT mice were cohoused with SFB-monoassociated NOD-SCID mice for 10 weeks (B) Litter and cage effect on ileitis development in SPF-housed *Tnf* $^{\Delta ARE}$ mice. Squares represent males; circles indicate females. Green, orange, and red symbols indicate *Tnf* $^{\Delta ARE}$ mice at 18-week endpoint with no (score 0), low (score <4) and high (score >4) ileitis histopathological score, respectively; grey symbols indicate WT littermates that do not develop ileitis; white symbols indicate male mice of unknown ileitis status. Each cage is delineated with the brackets below and a cage number. (C) Quantitative Analysis of SFB in recolonized *Tnf* $^{\Delta ARE}$ mice (F0, F1, F2). Color-code represents the severity of inflammation as described above. CT value >30 is regarded as non-specificity threshold. (D) Ileitis scores of recolonized 18-weeks-old *Tnf* $^{\Delta ARE}$ mice including 2 breeding generations (F0, F1, F2). Mice are color-coded based on inflammation severity with green (score 0); orange (score <4) (orange); and red (score >4). (E) Cladogram obtained from Linear discriminant analysis effect size (LEfSe) analysis of taxonomic profiling using 16S rRNA gene sequencing of intestinal microbiota in WT and *Tnf* $^{\Delta ARE}$ mice. (F) Comparison of relative abundance of bacterial genera between WT and *Tnf* $^{\Delta ARE}$ mice using LEfSe analysis. Taxa meeting an LDA significant threshold 2 are shown, taxa enriched in *Tnf* $^{\Delta ARE}$ mice (red) and taxa enriched in WT mice (blue). (G) Representative H&E-stained tissue sections from distal ileum, caecum, and proximal colon of *Tnf* $^{\Delta ARE}$ mice colonized with single bacterial strains

(*Alistipes*, *Lactobacillus murinus* and *E. coli LF82*) or with MIBAC, a minimal consortium of 7 bacterial strains showing no signs of inflammation. **Supplementary Figure S2.** Enhanced numbers of IL-17- and IFNg-expressing CD4-positive cells as well as neutrophilic granulocytes in inflamed mucosal tissue of *Tnf* $^{\Delta ARE}$ mice. Immune cells were isolated from spleen, MLN, and intestinal mucosa of jejunum, ileum, cecum, and colon of 12 weeks old *Tnf* $^{\Delta ARE}$ mice ($n = 3$) and WT controls ($n = 4$). (A) Quantitative analysis of *Ifng* transcript levels in mucosal tissue of distal ileum, cecum, and proximal colon from 4 and 12 weeks-old *Tnf* $^{\Delta ARE}$ mice and 12 weeks-old WT controls. Statistical significance was assessed by xy. *$p<0.05$; **$p<0.01$; ***$p<0.001$ was considered statistically significant. (B) Gating strategy used for the assessment of IL-17- and IFNg-expressing $CD3^+CD4^+$ immune cells. Discrimination of live and dead cell population was performed by applying specific fluorescent dye. Percentage of IL-17- (C) and IFNg- (D) expressing cells within the $CD3^+CD4^+$ population. (E) Gating strategy used for the assessment of neutrophilic granulocytes. Discrimination of live and dead cell population was performed by applying specific fluorescent dye. Population of neutrophils was identified by applying antibodies against CD45, CD11b, MHCII, Ly6C, and Ly6G. (F) Percentage of neutrophilic granulocytes was assessed within the $CD45^+CD11b^+$ population by gating for $MHCII^-Ly6C^{int}Ly6G^{high}$ cells. (G) Immunofluorescence staining of tissue sections from distal ileum of WT and *Tnf* $^{\Delta ARE}$ mice applying Ly6G and E-Cadherin. DAPI was used for nuclear visualization. (H) PAS-AB goblet cell staining in ileal tissue sections from 4 weeks and 12 weeks mono-colonized WT and *Tnf* $^{\Delta ARE}$ mice (400x). Lower panel represents higher magnification (1200x) of the indicated sections. Graph represents the quantification of goblet cells (x1000) in 1µm2 selected crypt area. Statistical analyses were performed by One-way analysis of variance (ANOVA) followed by Tukey test. *$p<0.05$; **$p<0.01$; ***$p<0.001$ was considered statistically significant. **Extended Supplementary Figure S2.** *B. adolescentis* monoassociation does not trigger inflammation *in Tnf* $^{\Delta ARE}$ *mice.* (A) Quantitative Analysis of *B.adolescentis* in recolonized *Tnf* $^{\Delta ARE}$ mice and WT control mice monoassociated with *B.adolescentis* for 4 weeks (B) Representative H&E-stained tissue sections from distal ileum, caecum, and colon of 12-week old ARE and WT control mice monoassociated with *B.adolescentis* for 4 weeks. (C) Tissue pathology scores of distal ileum (dI), caecum (CC), proximal colon (pC) and distal colon (dC) of *Tnf* $^{\Delta ARE}$ mice monoassociated with *B. adolescentis* for 4 weeks. (D) Quantitative analysis of Tnf, Il-17 and Ifng transcript levels in mucosal tissue of distal ileum from 12 weeks-old *Tnf* $^{\Delta ARE}$ mice mice monoassociated with *B. adolescentis* for 4 weeks. (E) Immunofluorescence (IF) co-staining of Lysozyme (red) and E-cadherin (IEC borders, blue) counterstained with Dapi (nuclei, cyan) in ileal tissue sections from 12 weeks-old *Tnf* $^{\Delta ARE}$ mice mice and their WT littermate controls monoassociated with *B. adolescentis* for 4 weeks (600x) lower panel: higher magnification of the indicated sections (3600x) and quantification of the total number of Lysozyme positive Paneth cells per crypt based on IF staining. Statistical analyses were performed by One-way analysis of variance (ANOVA) followed by Tukey test. **Supplementary Figure S3.** SFB initiate inflammation in humanized *Tnf* $^{\Delta ARE}$ mice. (A) *Tnf* $^{\Delta ARE}$ mice and WT controls were colonized either with fecal microbiota from CD patient only or in combination with SFB. Both groups were colonized at 8 weeks of age and assessed for tissue pathology at 12 weeks of age. (B) Severity of inflammation was assessed by evaluating the tissue pathology score in tissue sections of distal ileum, cecum and proximal colon of humanized or SFB + humanized *Tnf* $^{\Delta ARE}$ mice. (C) Quantitative analysis of SFB abundance in intestinal contents collected from ileal, colonic and cecal compartments of humanized or SFB + humanized *Tnf* $^{\Delta ARE}$ mice. (D) H&E-stained tissue sections of *Tnf* $^{\Delta ARE}$ mice revealed enhanced intestinal inflammation in the distal ileum and to a lower degree in cecum tissue of humanized *Tnf* $^{\Delta ARE}$ mice co-colonized with SFB. (E, F) Immunofluorescence (IF) co-staining of Lysozyme (red) and E-cadherin (IEC borders, blue) counterstained with Dapi (nuclei, cyan) in ileal tissue sections from *Tnf* $^{\Delta ARE}$ and WT mice colonized with human CD microbiota alone (hARE, hWT) or in co-colonization with SFB (hARE+SFB, hWT+SFB) (600x) lower panel: higher magnification of the indicated sections (3600x). Graph represents quantification of the total number of Lysozyme positive Paneth cells per crypt based on IF staining. Statistical analyses were performed by One-way analysis of variance (ANOVA) followed by Tukey test. (G) Beta-diversity analysis of bacterial community profiles in *Tnf* $^{\Delta ARE}$ and WT mice colonized with human CD microbiota alone (hARE, hWT) or in co-colonization with SFB (hARE+SFB, hWT+SFB) (H) Significantly increased percentage relative abundance of *Alistipes* and *Blautia* in humanized *Tnf* $^{\Delta ARE}$ and WT mice co-colonized with SFB (hARE+SFB, hWT+SFB). **Extended Supplementary Figure S3.** (A, B) Melting curves and CT values (C, D) Alignment to control human SFB sequence yielding 99% similarity. **Supplementary Figure S4.** (A) Correlation analysis between ileitis score and SFB abundance in cecal contents of chow-fed or PD-fed Specific pathogen-free (SPF) *Tnf* $^{\Delta ARE}$ mice and. (B) MDS analysis show separation of caecal bacterial communities according to diet among chow-fed WT, chow-fed or PD-fed *Tnf* $^{\Delta ARE}$ mice (C) Comparison of relative abundance of bacterial genera between SPF-housed *Tnf* $^{\Delta ARE}$ mice fed with chow or PD under SPF conditions, using LEfSe analysis. Taxa meeting an LDA significant threshold 2 are shown (D) Histopathology section of ileal and colonic tissue in ileal and colonic tissue of ex-GF *Tnf* $^{\Delta ARE}$ mice monocolonized with SFB and fed with chow or PD (E) Quantitative analysis of *Tnf* and *Il-17A* transcript levels in mucosal tissue of distal ileum from ex-GF *Tnf* $^{\Delta ARE}$ mice monocolonized with SFB and fed with chow or PD. PD: purified diet.

Additional file 2: Supplementary Table S1. Composition of chow, purified and fiber-rich diet. **Supplementary Table S2.** Description and metadata of patient mucosal biopsy samples screened for SFB presence. **Supplementary Table S3.** Minimal bacterial consortium (MIBAC) composition.

Acknowledgements
Not applicable.

Authors' contributions
D.H. conceived the study. A.Me, J.J, and N.W designed and performed mouse experiments and tissue analyses. SK and H.H performed tissue analysis. D.Hae and MA supported mouse experiments. A.Me performed 16S rRNA gene sequencing data analysis. A.Ma, A.S., L.Be, NH, MA, K.S, T.S, and J.P. provided patients samples. P.S, MB, AB, SZ, and F.C provided resources. A.Me and D.H. wrote the manuscript. All authors reviewed and approved the final manuscript.

Funding
Open Access funding enabled and organized by Projekt DEAL. Funded by the Deutsche Forschungsgemeinschaft (DFG, German Research Foundation)–project number 395357507 (SFB 1371, Microbiome Signatures) and ANR JCJC grant MicroEducation and Bill and Melinda Gates Grand Challenge grant to PS.

Availability of data and materials
The demultiplexed reads for 16S amplicon sequencing datasets from gnotobiotic humanized mice have been deposited to the NCBI Sequence Read Archive [http://www.ncbi.nlm.nih.gov/sra] under the accession no. PRJNA873788.

Declarations

Ethics approval and consent to participate
The ethical statements regarding the animal experimentation are included in the "Materials and methods" section.

Consent for publication
Not applicable.

Competing interests
The authors declare that they have no competing interests.

Author details
[1]Chair of Nutrition and Immunology, Technical University of Munich, Freising, Germany. [2]APHP, Hôpital Saint Louis, Department of Gastroenterology, INSERM UMRS 1160, Paris Diderot, Sorbonne Paris-Cité University, Paris, France. [3]Université Paris Cité, INSERM U1160, EMiLy, Institut de Recherche Saint-Louis, Paris, France. [4]Department of Experimental Pathology, Instituto de Investigaciones Biomédicas de Barcelona CSIC, IDIBAPS, CIBERehd, Barcelona, Spain.

[5]Department of Pediatrics, Dr. von Hauner Children's Hospital, University Hospital, LMU Munich, Munich, Germany. [6]Hannover Medical School, Institute for Laboratory Animal Science, Hannover, Germany. [7]Department of Medicine I, University Hospital Dresden, Technische Universität (TU) Dresden, Dresden, Germany. [8]Université Paris Cité, INSERM UMR-S1151, CNRS UMR-S8253, Institut Necker Enfants Malades, F-75015 Paris, France. [9]Digestive Health Research Institute, Case Western Reserve University School of Medicine, Cleveland, OH, USA. [10]ZIEL-Institute for Food and Health, Technical University of Munich, Freising, Germany.

Received: 24 August 2022 Accepted: 25 February 2023
Published online: 31 March 2023

References

1. Kaplan GG. The global burden of IBD: from 2015 to 2025. Nat Rev Gastroenterol Hepatol. 2015;12:720–7.
2. Renz H, et al. Gene-environment interactions in chronic inflammatory disease. Nat Immunol. 2011;12:273.
3. Franke A, et al. Genome-wide meta-analysis increases to 71 the number of confirmed Crohn's disease susceptibility loci. Nat Genet. 2010;42:1118–25.
4. De Lange, K.M.,L. M. C. B. Genome-wide association study implicates immune activation of multiple integrin genes in inflammatory bowel disease. Nat Genet. 2017; 49:256–261.
5. Graham DB, Xavier RJ. Pathway paradigms revealed from the genetics of inflammatory bowel disease. Nature. 2020;578:527–39.
6. Jostins L, et al. Host-microbe interactions have shaped the genetic architecture of inflammatory bowel disease. Nature. 2012;491:119–24.
7. Liu JZ, Van Sommeren S, Huang H, Ng SC, Alberts R. Europe PMC Funders Group Association analyses identify 38 susceptibility loci for inflammatory bowel disease and highlight shared genetic risk across populations. Nat Genet. 2015;47:979–86.
8. Kamada N, Seo S-U, Chen GY, Núñez G. Role of the gut microbiota in immunity and inflammatory disease. Nat Rev Immunol. 2013;13:321–35.
9. McIlroy J, Ianiro G, Mukhopadhya I, Hansen R, H. G. Review article : the gut microbiome in inflammatory bowel disease — avenues for microbial management. Aliment Pharmacol Ther. 2018;26–42. https://doi.org/10.1111/apt.14384.
10. Levy M, Kolodziejczyk AA, Thaiss CA, Elinav E. Dysbiosis and the immune system. Nat Rev Immunol. 2017;17:219–32.
11. Metwaly A, Reitmeier S, Haller D. Microbiome risk profiles as biomarkers for inflammatory and metabolic disorders. Nat Rev Gastroenterol Hepatol. 2022;19:383–97.
12. Schaubeck M, et al. Dysbiotic gut microbiota causes transmissible Crohn's disease-like ileitis independent of failure in antimicrobial defence. Gut. 2016;65:225–37.
13. Roulis M, et al. Host and microbiota interactions are critical for development of murine Crohn's-like ileitis. Mucosal Immunol. 2016;9:787–97.
14. Rehaume LM, et al. ZAP-70 genotype disrupts the relationship between microbiota and host, leading to spondyloarthritis and ileitis in SKG mice. Arthritis Rheumatol (Hoboken, NJ). 2014;66:2780–92.
15. Metwaly A, et al. Integrated microbiota and metabolite profiles link Crohn's disease to sulfur metabolism. Nat Commun. 2020;11:4322.
16. Lengfelder I, et al. Complex bacterial consortia reprogram the colitogenic activity of enterococcus faecalis in a gnotobiotic mouse model of chronic, immune-mediated colitis. Front Immunol. 2019;10:1420.
17. Kontoyiannis D, Pasparakis M, Pizarro TT, Cominelli F, Kollias G. Impaired on/off regulation of TNF biosynthesis in mice lacking TNF AU-rich elements: implications for joint and gut-associated immunopathologies. Immunity. 1999;10:387–98.
18. Cominelli F, Arseneau KO, Rodriguez-Palacios A, Pizarro TT. Uncovering pathogenic mechanisms of inflammatory bowel disease using mouse models of Crohn's disease-like ileitis: what is the right model? Cell Mol Gastroenterol Hepatol. 2017;4:19–32.
19. Buttó LF, Schaubeck M, Haller D. Mechanisms of microbe-host interaction in Crohn's disease: Dysbiosis vs. Pathobiont Selection. Front Immunol. 2015. https://doi.org/10.3389/fimmu.2015.00555.
20. Ahmed M, Metwaly A, Haller D. Modeling microbe-host interaction in the pathogenesis of Crohn's disease. Int J Med Microbiol. 2021;311:151489.
21. Al Nabhani Z, et al. A weaning reaction to microbiota is required for resistance to immunopathologies in the adult. Immunity. 2019;50:1276–1288.e5.
22. Gaboriau-Routhiau V, et al. The key role of segmented filamentous bacteria in the coordinated maturation of gut helper T cell responses. Immunity. 2009;31:677–89.
23. Lécuyer E, et al. Segmented filamentous bacterium uses secondary and tertiary lymphoid tissues to induce gut IgA and specific T helper 17 cell responses. Immunity. 2014;40:608–20.
24. Schnupf P, et al. Growth and host interaction of mouse segmented filamentous bacteria in vitro. Nature. 2015;520:99–103.
25. Snel J, et al. Interactions between gut-associated lymphoid tissue and colonization levels of indigenous, segmented, filamentous bacteria in the small intestine of mice. Can J Microbiol. 1998;44:1177–82.
26. Klaasen HL, et al. Intestinal, segmented, filamentous bacteria in a wide range of vertebrate species. Lab Anim. 1993;27:141–50.
27. Caselli M, Tosini D, Gafà R, Gasbarrini A, Lanza G. Segmented filamentous bacteria-like organisms in histological slides of ileo-cecal valves in patients with ulcerative colitis. Am J Gastroenterol. 2013;108(5):860–1. https://doi.org/10.1038/ajg.2013.61.
28. Yin Y, et al. Comparative analysis of the distribution of segmented filamentous bacteria in humans, mice and chickens. ISME J. 2013;7:615–21.
29. Jonsson H. Segmented filamentous bacteria in human ileostomy samples after high-fiber intake. FEMS Microbiol Lett. 2013;342:24–9.
30. Finotti A, Gasparello J, Lampronti I, Cosenza LC, Maconi G, Matarese V, Gentili V, Di Luca D, Gambari R, Caselli M. PCR detection of segmented filamentous bacteria in the terminal ileum of patients with ulcerative colitis. BMJ Open Gastroenterol. 2017;4(1):e000172.https://doi.org/10.1136/bmjgast-2017-000172.
31. Atarashi K, et al. Th17 cell induction by adhesion of microbes to intestinal epithelial cells. Cell. 2015;163:367–80.
32. Ivanov II, et al. Induction of intestinal Th17 cells by segmented filamentous bacteria. Cell. 2009;139:485–98.
33. Salzman NH. Paneth cell defensins and the regulation of the microbiome: détente at mucosal surfaces. Gut Microbes. 2010;1:401–6.
34. Chen B, et al. Presence of segmented filamentous bacteria in human children and its potential role in the modulation of human gut immunity. Front Microbiol. 2018;9:1403.
35. Schaubeck M, Haller D. Reciprocal interaction of diet and microbiome in inflammatory bowel diseases. Curr Opin Gastroenterol. 2015;31:464–70.
36. Khalili H, et al. The role of diet in the aetiopathogenesis of inflammatory bowel disease. Nat Rev Gastroenterol Hepatol. 2018;15:525–35.
37. Ananthakrishnan AN, et al. Long-term intake of dietary fat and risk of ulcerative colitis and Crohn{\textquoteright}s disease. Gut. 2014;63:776–84.
38. Racine A, et al. Dietary patterns and risk of inflammatory bowel disease in Europe: results from the EPIC Study. Inflamm Bowel Dis. 2016;22:345–54.
39. Klaasen HLBM, Koopman JP, Van Den Brink ME, Scholten PM, Beynen AC. Influence of macronutrients on segmented filamentous bacteria in the small intestine of mice. Microb Ecol Health Dis. 1991;4:47–51.
40. Koopman JP, Kennis HM, Nouws JF, Morse H. Evidence for antibacterial substances in diets for laboratory animals. Z Versuchstierkd. 1986;28:179–86.
41. Koopman JP, Kennis HM, Nouws JF, Hectors MP, Nagengast F. Influence of different laboratory animal diets on segmented organisms in the small intestine, relative cecal weight, fecal Enterobacteriaceae and bile acid excretion. Z Versuchstierkd. 1987;29:93–7.
42. Corraliza AM, et al. Differences in peripheral and tissue immune cell populations following haematopoietic stem cell transplantation in Crohn's disease patients. J Crohns Colitis. 2019;13:634–47.
43. Jauregui-Amezaga A, et al. Improving safety of autologous haematopoietic stem cell transplantation in patients with Crohn's disease. Ann Rheum Dis. 2016;75:1661–6.
44. López-García A, et al. Autologous haematopoietic stem cell transplantation for refractory crohn's disease: Efficacy in a single-centre cohort. J Crohns Colitis. 2017. https://doi.org/10.1093/ecco-jcc/jjx054.
45. Berry D, Mahfoudh KB, Wagner M, Loy A. Barcoded primers used in multiplex amplicon pyrosequencing bias amplification. Appl Environ Microbiol. 2011;77:7846–9.
46. Edgar RC. UPARSE: highly accurate OTU sequences from microbial amplicon reads. Nat Methods. 2013;10(10):996–8. https://doi.org/10.1038/nmeth.2604.

47. Edgar RC. UNOISE2: improved error-correction for Illumina 16S and ITS amplicon sequencing. bioRxiv. 2016;81257. https://doi.org/10.1101/081257.
48. Yilmaz P, et al. The SILVA and 'all-species Living Tree Project (LTP)' taxonomic frameworks. Nucleic Acids Res. 2014;42:643–8.
49. Lagkouvardos I, Fischer S, Kumar N, Clavel T. Rhea : a transparent and modular R pipeline for microbial profiling based on 16S rRNA gene amplicons. PeerJ. 2017. https://doi.org/10.7717/peerj.2836.
50. Prakash T, et al. Complete genome sequences of rat and mouse segmented filamentous bacteria, a potent inducer of Th17 cell differentiation. Cell Host Microbe. 2011;10:273–84.
51. Suzuki K, et al. Aberrant expansion of segmented filamentous bacteria in IgA-deficient gut. Proc Natl Acad Sci. 2004;101:1981 LP–986.
52. Shukla R, Ghoshal U, Dhole TN, Ghoshal UC. Fecal microbiota in patients with irritable bowel syndrome compared with healthy controls using real-time polymerase chain reaction: an evidence of dysbiosis. Dig Dis Sci. 2015;60:2953–62.
53. Jonsson H, Hugerth LW, Sundh J, Lundin E, Andersson AF. Genome sequence of segmented filamentous bacteria present in the human intestine. Commun Biol. 2020;3:485.
54. Snel J, et al. Comparison of 16S rRNA sequences of segmented filamentous bacteria isolated from mice, rats, and chickens and proposal of 'Candidatus Arthromitus'. Int J Syst Bacteriol. 1995;45:780–2.
55. Erben U, et al. Original Article A guide to histomorphological evaluation of intestinal inflammation in mouse models. Int J Clin Exp Pathol. 2014;7:4557–76.
56. Katakura K, et al. Toll-like receptor 9-induced type I IFN protects mice from experimental colitis. *J Clin Invest*. 2005;115:695–702.
57. Pizarro TT, et al. SAMP1/YitFc mouse strain: a spontaneous model of Crohn's disease-like ileitis. Inflamm Bowel Dis. 2011;17:2566–84.
58. Lagkouvardos I, et al. The mouse intestinal bacterial collection (miBC) provides host-specific insight into cultured diversity and functional potential of the gut microbiota. Nat Microbiol. 2016;1:16131.
59. Tan TG, et al. Identifying species of symbiont bacteria from the human gut that, alone, can induce intestinal Th17 cells in mice. Proc Natl Acad Sci. 2016;113:E8141 LP–E8150.
60. Ericsson AC, et al. Isolation of segmented filamentous bacteria from complex gut microbiota. Biotechniques. 2015;59:94–8.
61. Sartor RB, Wu GD. Roles for intestinal bacteria, viruses, and fungi in pathogenesis of inflammatory bowel diseases and therapeutic approaches. Gastroenterology. 2017;152:327–339.e4.
62. Nagao-Kitamoto H, Kamada N. Host-microbial cross-talk in inflammatory bowel disease. Immune Netw. 2017. https://doi.org/10.4110/in.2017.17.1.1.
63. Morgan XC, et al. Dysfunction of the intestinal microbiome in inflammatory bowel disease and treatment. Genome Biol. 2012;13:R79.
64. Darfeuille-Michaud A, et al. High prevalence of adherent-invasive Escherichia coli associated with ileal mucosa in Crohn's disease. Gastroenterology. 2004;127:412–21.
65. Prindiville TP, et al. Bacteroides fragilis enterotoxin gene sequences in patients with inflammatory bowel disease. Emerg Infect Dis. 2000;6:171–4.
66. Gálvez J. Role of Th17 cells in the pathogenesis of human IBD. ISRN Inflamm. 2014;2014:928461.
67. Johansson MEV, et al. Normalization of host intestinal mucus layers requires long-term microbial colonization. Cell Host Microbe. 2015;18:582–92.
68. Moschen AR, et al. Lipocalin 2 protects from inflammation and tumorigenesis associated with gut microbiota alterations. Cell Host Microbe. 2016;19:455–69.
69. Goetz DH, et al. The neutrophil lipocalin NGAL is a bacteriostatic agent that interferes with siderophore-mediated iron acquisition. Mol Cell. 2002;10:1033–43.
70. Werner T, et al. Depletion of luminal iron alters the gut microbiota and prevents Crohn's disease-like ileitis. Gut. 2011;60:325 LP – 333.
71. Sczesnak A, et al. The genome of th17 cell-inducing segmented filamentous bacteria reveals extensive auxotrophy and adaptations to the intestinal environment. Cell Host Microbe. 2011;10:260–72.
72. Schnupf P, Gaboriau-Routhiau V, Cerf-Bensussan N. Host interactions with Segmented Filamentous Bacteria: an unusual trade-off that drives the post-natal maturation of the gut immune system. Semin Immunol. 2013;25:342–51.
73. Stepankova R, et al. Segmented filamentous bacteria in a defined bacterial cocktail induce intestinal inflammation in SCID mice reconstituted with CD45RBhigh CD4+ T cells. Inflamm Bowel Dis. 2007;13:1202–11.
74. Flannigan KL, et al. IL-17A-mediated neutrophil recruitment limits expansion of segmented filamentous bacteria. Mucosal Immunol. 2017;10:673–84.
75. Bhaumik S, Basu R. Cellular and molecular dynamics of Th17 differentiation and its developmental plasticity in the intestinal immune response. Front Immunol. 2017;8:254.
76. Hueber W, et al. Secukinumab, a human anti-IL-17A monoclonal antibody, for moderate to severe Crohn's disease: unexpected results of a randomised, double-blind placebo-controlled trial. Gut. 2012;61:1693–700.
77. Ghoreschi K, et al. Generation of pathogenic T(H)17 cells in the absence of TGF-β signalling. Nature. 2010;467:967–71.
78. Lee Y, et al. Induction and molecular signature of pathogenic TH17 cells. Nat Immunol. 2012;13:991–9.
79. Omenetti S, et al. The intestine harbors functionally distinct homeostatic tissue-resident and inflammatory Th17 cells. Immunity. 2019;51:77–89.e6.
80. Nagao-Kitamoto H, et al. Functional characterization of inflammatory bowel disease-associated gut dysbiosis in gnotobiotic mice. CMGH. 2016. https://doi.org/10.1016/j.jcmgh.2016.02.003.
81. Bolsega S, Basic M, Smoczek A, Buettner M, Eberl C, Ahrens D, Odum KA, Stecher B, Bleich A. Composition of the Intestinal Microbiota Determines the Outcome of Virus-Triggered Colitis in Mice. Front Immunol. 2019;23(10):1708. https://doi.org/10.3389/fimmu.2019.01708.
82. Schwerd T, et al. Exclusive enteral nutrition in active pediatric Crohn disease: Effects on intestinal microbiota and immune regulation. J Allergy Clin Immunol. 2016;138:592–6.
83. Gerasimidis K, Nikolaou CK, Edwards CA, McGrogan P. Serial fecal calprotectin changes in children with Crohn's disease on treatment with exclusive enteral nutrition: associations with disease activity, treatment response, and prediction of a clinical relapse. J Clin Gastroenterol. 2011;45:234–9.
84. Klaasen HL, Koopman JP, van den Brink ME, Bakker MH, Beynen AC. Influence of a natural-ingredient diet containing Phaseolus vulgaris on the colonization by segmented, filamentous bacteria of the small bowel of mice. Int J Vitam Nutr Res. 1992;62:334–41.
85. Brotherton CS, Martin CA, Long MD, Kappelman MD, Sandler RS. Avoidance of fiber is associated with greater risk of Crohn's disease flare in a 6-month period. Clin Gastroenterol Hepatol Off Clin Pract J Am Gastroenterol Assoc. 2016;14:1130–6.
86. Desai MS, et al. A dietary fiber-deprived gut microbiota degrades the colonic mucus barrier and enhances pathogen susceptibility. Cell. 2016;167:1339–1353.e21.
87. Luceri C, et al. Effect of butyrate enemas on gene expression profiles and endoscopic/histopathological scores of diverted colorectal mucosa: a randomized trial. Dig liver Dis Off J Ital Soc Gastroenterol Ital Assoc Study Liver. 2016;48:27–33.
88. Pereira GV, et al. Unravelling specific diet and gut microbial contributions to inflammatory bowel disease. bioRxiv. 2022;2022.04.03.486886. https://doi.org/10.1101/2022.04.03.486886.
89. Armstrong HK, et al. Unfermented β-fructan fibers fuel inflammation in select inflammatory bowel disease patients. Gastroenterology. 2023. https://doi.org/10.1053/j.gastro.2022.09.034.

Publisher's Note